Acoustic and psychoacoustic characterisation of small-scale contra-rotating propellers

Fabio Casagrande Hirono *, James Robertson, Antonio J. Torija Martinez

School of Science, Engineering and Environment, University of Salford, Manchester M5 4WT, United Kingdom

A R T I C L E   I N F O

A B S T R A C T

This paper reports an experimental investigation of noise radiation and psychoacoustic evaluation of contra-rotating propellers with different blade counts over multiple emission angles and thrust settings. A series of aeroacoustic and psychoacoustic tests were performed with a contra-rotating propeller rig at the University of Salford, UK, where both propellers' blade count and their axial separation z were varied at static conditions and constant thrust. The sounds were analysed using conventional acoustic metrics, such as Sound Pressure Level (SPL) and Sound Power Level for tonal, broadband, and overall noise, and using the psychoacoustic Sound Quality Metrics (SQMs) Loudness, Fluctuation Strength, Roughness, Tonality, and Impulsiveness. Configurations with axial separation-to-diameter ratio z/D between 0.2–0.4 exhibited a balance between tonal and broadband noise generation mechanisms, resulting in reduced noise levels and reduced annoyance for on-axis observers. The number of blades played a secondary role on determining noise levels: higher blade counts resulted in lower overall noise levels at larger axial separations, although at shorter distances ($z/D < 0.2$) increasing the blade count led to higher noise levels. The SQMs Loudness, Fluctuation Strength, and Tonality were found to also reach a minimum at $z/D = 0.3$, although increasing the number of propeller blades led to a decrease in Loudness but not in Fluctuation Strength and Tonality. The dominant noise generation mechanisms observed here present a directivity null perpendicular to the propellers' axis, and no clear trends were observed for acoustic and psychoacoustic metrics at this emission angle. A listening experiment was set up to validate the results of the acoustic and psychoacoustic analysis, and its results suggest that the reported noise annoyance is driven by Loudness, Fluctuation Strength and Tonality metrics ($p < 0.01$) at on-axis radiation, while at 90° emission angle, Loudness ($p < 0.01$) and Tonality ($p < 0.05$) are the main contributors to noise annoyance.

1. Introduction

In recent years, overlapping counter- and contra-rotating propellers have gained renewed interest as potential propulsion systems for novel electric aircraft, such as Unmanned Aerial Vehicles (UAVs). When compared to single propellers, contra-rotating systems could achieve improved aerodynamic efficiency at reduced sizes and add redundant control to ensure flight safety in case of component failure [1,2]. However, it is generally accepted that new aircraft must be significantly quieter than current conventional ones to gain public acceptance and be commercially viable [3].

* Corresponding author.
  E-mail addresses: fchirono@gmail.com (F. Casagrande Hirono), J.Robertson6@edu.salford.ac.uk (J. Robertson), A.J.TorijaMartinez@salford.ac.uk (A.J. Torija Martinez).

The noise radiated by contra-rotating propeller configurations has been the subject of active research in aeroacoustics for decades [4,5]. An important characteristic of overlapping propellers is their significant aerodynamic interactions, which can result in high noise emissions when not carefully designed [6]. In particular, very high amplitude tones are radiated when propellers are mounted at short axial spacings, increasing perceived annoyance to aircraft noise [7].

In a contra-rotating configuration, tonal noise is generated at multiple sum and difference tones by potential field interactions between both propellers when these are closely spaced [8,9], and by unsteady loading on the downstream propeller due to viscous wake and tip vortex interaction at various axial distances [1,9,10]. Interaction tones tend to dominate the noise radiation for near-axis emission angles [1,8,9], and are generally considered the most important noise source to be tackled in contra-rotating systems. As the potential field decays exponentially away from the propeller plane, increasing the axial spacing z between the propellers is an effective tool to reduce potential field interaction tones. On the other hand, larger axial separations lead to increased broadband noise due to interaction of the downstream rotor with the convecting and spreading tip vortex and turbulent wake from the upstream rotor [11].

Due to the contrasting nature of the various noise generation mechanisms within a contra-rotating propeller system, there is a possibility for finding a balance between the multiple noise sources. McKay et al. [1] showed that increasing axial spacing z up to approximately $0.2D$, where the propellers' diameter D varied between 12 and 15 in., in a two-bladed contra-rotating propeller system reduced the magnitude of zero-azimuthal order interaction tones without a significant change to broadband noise for an on-axis observer, but they did not investigate larger separation distances. Torija et al. [7] and Chaitanya et al. [9] investigated the Sound Power Level (PWL) radiated from a two-bladed contra-rotating rotor, and proposed optimal axial spacings z/D of 0.2–0.4 and 0.25 respectively. At this optimum spacing, the dominant noise source mechanisms contribute equally to the overall sound power [9]. Although McKay et al. [1] also investigated the noise from a three-bladed contra-rotating propeller configuration, neither work investigated higher blade counts.

While current understanding of aircraft noise provides a solid foundation to analyse noise generation mechanisms in novel electric aircraft, their wide range of configurations also brings new challenges [3]. One example is distributed propulsion, which opens more opportunities for undesired noise-generation interactions. Established aircraft noise certification metrics do not account for the distinctive noise characteristics of novel vehicles and designs, and might not accurately reflect human perception of these sounds [7,12]. More recently, perception-influenced design approaches [12] have used psychoacoustics-based evaluation and optimisation methods to better understand and reduce the noise impact of both conventional and novel rotor and propeller arrangements [7,13–15].

Torija et al. [15] conducted a psychoacoustic evaluation of a series of sounds of small-scale contra-rotating two-bladed propellers with 14, 16, and 18-in. diameter rotors. Investigating the annoyance reported by participants of a listening experiment as a function of the rotor–rotor axial spacing, the authors found an optimum axial spacing of $z/D = 0.1$ for the 14-in. diameter rotor, and $z/D = 0.2$–0.4 for 16- and 18-in. rotors. These results suggest differences in the amplitude of potential field interactions as a function of rotor–rotor axial spacing for different blade diameters. This poses the question of how other configurations, e.g., with varying blade numbers, will influence potential fields and other noise sources in contra-rotating propellers.

In general, investigations published so far in both aeroacoustics and psychoacoustics of small-scale contra-rotating propellers generally used only two or three blades per propeller, and some cases considered only a small range of normalised axial separation distances z/D. In a preliminary investigation, the authors of this paper investigated the effects of varying the number of blades (between 2 and 6) and the axial spacing on the on-axis noise emissions of the contra-rotating rig described herein, operating at constant thrust [16]. The results followed the trends previously observed in the literature, with a general decrease in noise radiation at axial separations near $z/D = 0.3$ for all blade counts, when tonal and broadband sources show almost identical levels, and a slight decrease in noise with larger blade counts. As part of the same investigation, a psychoacoustic analysis of the same recordings using the Sound Quality Metrics (SQMs) Loudness, Tonality, and Impulsiveness showed that loudness and tonality also exhibit a minima for axial spacing near $z/D = 0.3$, but only small variations were observed on both metrics for changes in blade number. On the other hand, impulsiveness generally increased with axial spacing, and no clear trend was determined for changes in blade number.

The goal of this paper is to extend previous contributions on noise from contra-rotating propellers for small-scale UAVs,[1] and further investigate the effects of varying numbers of propeller blades and rotor axial spacing on noise radiation at multiple observer directions. The overall sound spectra are decomposed into their tonal and broadband contributions, and the trade-offs between these two noise components are investigated to find optimal rotor configurations. Different emission angles are shown to exhibit dissimilar trends in noise metrics, therefore the Sound Power Level PWL is also used to quantify the sound radiation over the entire domain surrounding the propellers. The PWL is shown to perform well as a global optimisation metric for contra-rotating propeller noise.

The recorded sounds are also analysed in terms of the Sound Quality Metrics Loudness, Fluctuation Strength, Roughness, Tonality, and Impulsiveness. These metrics were found in Torija et al. [7,15] to better describe the changes in potential field interactions as a function of axial spacing. In addition, a listening experiment was conducted to investigate the effect of the number of propeller blades, rotor axial spacing, thrust, and emission angle on perceived noise annoyance. Participants were asked to rate the annoyance of a selection of test sounds relative to a reference sound, and the test results are explained using the conventional acoustic metrics and Sound Quality Metrics presented above.

---

[1] The Federal Aviation Administration (FAA) rule 14 CFR Part 107 defines small unmanned aircraft systems (UAS) as those weighing less than 55 pounds.

Table 1
Summary of propeller characteristics used in the experiments.

Diameter D [m]	Propeller pitch [m]	Blade chord at $0.75 R_{tip}$ [m]
0.28	0.178	0.025

1.1. Overview of noise generation mechanisms

This section briefly describes the expected noise generation mechanisms for a contra-rotating propeller system and their characteristics. For more details, the reader is referred to Greenwood et al. [3] for a thorough overview of rotor noise sources, and to Chaitanya et al. [9] for a detailed discussion on rotor–rotor interaction noise sources. Following the taxonomies made in the above mentioned references, the main sources of noise in a contra-rotating propeller rig can be divided into: (1) rotor-alone noise, generated by each propeller in isolation; (2) installation noise, due to interactions of the propellers with their mounting structures; and (3) rotor–rotor interaction noise, which is the focus of the present work.

Rotor-alone noise at low Mach numbers consists of tonal noise arising from blade thickness and blade steady loading, and broadband noise from nondeterministic loading — mainly turbulent boundary layer-trailing edge noise at low Reynolds numbers [17–19]. The tonal components typically dominate the spectrum at low to mid frequencies and decrease in amplitude at higher frequencies, whereas the broadband component dominates the spectrum at higher frequencies [1,8]. In a contra-rotating configuration, these noise sources will exist independently for each rotor, and are generally not affected by the presence of the adjacent rotor or their axial separation [1,20]. Thickness noise and steady loading noise are generally stronger for observers on the rotor plane due to convective amplification, although thickness noise is typically negligible at very low Mach numbers [3]. Broadband noise has a dipole directivity pattern, with a null on the rotor plane and stronger radiation towards the propeller axis.

In an assessment of single rotors at low Reynolds numbers, Gojon et al. [19] observed a significant decrease in the amplitude of the Blade-Passing Frequency (BPF) noise when increasing the number of rotor blades from 2 to 5 at constant thrust. This reduction was more pronounced on the rotor plane, and was mainly due to the reduced blade loading and rotational speed required to achieve the same thrust at higher blade counts. The reduction in tonal noise was counterbalanced by a slight increase in broadband noise with increasing blade count at all emission angles. The combined effects lead to a reduction in Overall Sound Pressure Level (OASPL) of about 10 dB on the rotor plane at higher blade counts, and an almost constant OASPL at emission angles away from the rotor plane ($\pm 60°$) at all blade counts.

Installation noise is caused by interactions between the rotating blades and fixed rig mounting struts, generating additional unsteady loading forces on the rotors due to stationary flow distortions, and unsteady loading on the fixed components due to interactions with the moving blades. Mounting struts or booms can shed wakes containing both large-scale coherent structures and short-scale nondeterministic structures, generating additional tonal and broadband noise when interacting with the propeller blades. The fixed components can also add acoustic scattering and reflections. As these noise sources will depend on the geometry, size and placement of the fixed components, they are generally specific to a particular experimental setup, and can be difficult to isolate after setting up the experiment. Installation effects share similar characteristics to rotor-airframe interaction noise on aircrafts [3].

Finally, rotor–rotor interaction noise is caused by periodic unsteady loading forces generated on each propeller by interaction with the flowfield of the adjacent contra-rotating propeller [1,9,21], and are highly sensitive to propeller axial separation. Loading forces can arise on the downstream propeller due to interactions with the tip vortex, viscous wakes, and bound potential field of the upstream propeller, whereas loading forces on the upstream propeller are due to interactions with the bound potential field of the downstream propeller. Potential field interaction is the dominant source of tonal noise due to unsteady loading on closely-spaced propellers, but decays exponentially with increasing propeller axial separation [4,9]. At medium distances, near-wake and tip vortex interactions become the main source of rotor–rotor interaction tonal noise [1,4,9], although the dominant source mechanism at each distance is currently unclear.

McKay et al. [1] proposed an analytical model to describe tonal noise generated by rotor–rotor interactions. Their model showed that the azimuthal mode order $\nu = n_2 B_2 - n_1 B_1$, where the subscripts 1,2 denote the upstream and downstream propeller respectively, n_1, n_2 are integers, and B_1, B_2 are the number of blades, has a strong effect on the directionality of the interaction tone occurring at frequency $\omega_{n_1,n_2} = n_1 B_1 \Omega_1 + n_2 B_2 \Omega_2$: for an observer on-axis, tones with azimuthal order $\nu = 0$ will display a much higher magnitude than tones with non-zero azimuthal order. The reverse trend applies for an in-plane observer, where interaction tones with non-zero azimuthal order and rotor-alone tones are more prominent. Assuming both propellers have the same number of blades ($B_1 = B_2 = B$) and rotational speeds ($\Omega_1 = \Omega_2 = \Omega$), as is the case here, the strongest on-axis tones will be those where $n_1 = n_2$, which occur at frequencies $\omega_n = 2nB\Omega$ that are even-order harmonics of the Blade Passing Frequency $\omega_{BPF} = B\Omega$.

As the upstream propeller viscous wake develops and the turbulence lengthscale growths within the rotor–rotor axial separation distance, noise generated by wake interaction and tip vortex interaction can change in character from tonal noise at near distances to nondeterministic narrowband noise (or fully broadband noise) noise at larger distances [9]. Nondeterministic narrowband noise is characterised by broad spectral peaks around the BPF and its harmonics. Chaitanya et al. [9] showed experimental evidence of an increase in the size of the upstream rotor tip vortex with increasing distance, resulting in increased low-frequency broadband noise from interaction with the downstream rotor.

Table 2
Mean rotational frequencies f_{shaft}, blade tip Mach numbers M_{tip}, and thrust coefficients $C_T = T/\rho A V_{\text{tip}}^2$ per thrust-blade number configuration.

N_{blades}	4 N thrust			8 N thrust		
	f_{shaft} [Hz]	M_{tip}	C_T	f_{shaft} [Hz]	M_{tip}	C_T
2	56.9	0.147	0.0213	78.4	0.203	0.0222
3	49.6	0.128	0.0278	69.6	0.180	0.0280
4	45.0	0.116	0.0340	61.9	0.160	0.0354
5	42.3	0.104	0.0388	55.8	0.151	0.0397
6	40.3	0.104	0.0420	55.8	0.144	0.0435

1.2. Paper organisation

The paper is organised as follows: the experimental setup and acoustic measurement procedures are discussed in Section 2, and its results are shown in Section 3. The psychoacoustic analysis and the listening experiment are explained in Section 4, and its results in Section 5. The paper then summarises the findings in Section 6.

2. Aeroacoustic measurements

The aeroacoustic measurements were carried out in the Anechoic Chamber of the University of Salford, UK. The anechoic chamber has a lower cutoff frequency of 100 Hz, background noise level of -12.4 dB(A), and a working space of $5.4 \times 4.1 \times 3.3$ m.[2]

2.1. Contra-rotating test rig

A custom-made contra-rotating propeller rig was designed and built in the Acoustics Research Centre (ARC), University of Salford. It consists of two *Turnigy Aerodrive SK3 - 3542-800* brushless motors mounted on a steel and aluminium frame. The blades used are off-the-shelf *Flightline 12 × 7*, with 12-in. (approx. 0.3 m) propeller diameter and 7-in. (approx. 0.178 m) pitch, in both forward and reverse configuration. The blades were installed in a fixed-pitch configuration, and their tips were trimmed for use in a separate experiment, resulting in a rotor diameter $D = 0.28$ m. The propeller characteristics are summarised in Table 1.

A set of custom-made hubs allowed changing the number of blades on each rotor. For the present study, both rotors were operated with the same number of blades. Measurements were taken with 2, 3, 4, 5, and 6 blades, and the mean shaft frequencies $f_{\text{shaft}} = \Omega_{\text{shaft}}/2\pi$, blade tip Mach numbers $M_{\text{tip}} = V_{\text{tip}}/c_0$ (where $V_{\text{tip}} = \Omega_{\text{shaft}} R_{\text{tip}}$ is the blade tip speed, and c_0 is the speed of sound, both in m/s), and thrust coefficient $C_T = T/\rho A V_{\text{tip}}^2$ (where T is the mean thrust in Newtons, $A = \pi R_{\text{tip}}^2$ is the rotor disk area in m^2, and ρ is the air density in kg/m^3) for each thrust/blade number combination are shown in Table 2. Configurations with lower blade counts required slightly higher shaft frequencies to achieve the same thrust, and the equivalent blade tip Mach numbers ranged from $M_{\text{tip}} \approx 0.14$ for six blades to $M_{\text{tip}} \approx 0.2$ for two blades for 8 N thrust, and $M_{\text{tip}} \approx 0.1$ to $M_{\text{tip}} \approx 0.15$ for 4 N thrust. The thrust coefficient C_T is very similar for propellers with identical number of blades, as expected for a zero-inflow case. The process for estimating f_{shaft} from the acoustic data is described further below.

The motors were attached to axles, which in turn were attached to moving stands mounted on railings. This allowed alteration of the rotor axial separation distance z along the rails of the frame, ranging from $0.1D$ to $1.0D$. Measurements were taken at $z/D = 0.1$, 0.2, 0.3, 0.4, 0.6, 0.8, and 1.0. For a fixed number of blades, the rotational frequency required to achieve a target thrust force was not affected by rotors' axial separation. The assembled rig is shown in Fig. 1(a). A single servo tester was connected to two *Maytech MT40A-OPTO-SF32* Electronic Speed Controllers (ESC), and each ESC was connected to one motor. The ESCs were operated from a power strip connected to mains voltage. Although both propellers' rotational speeds were nominally identical for all configurations, in practice they varied very slightly due to the open-loop characteristic of the control system and small imperfections between the two motors and propellers, as discussed below.

The aluminium framework was mounted on a steel rod, held through the middle by a pivot point screw. A *RDP Group RLT0010Kg* S-type load cell was installed between steel rod and a main shaft attached to the anechoic chamber floor, and is able to measure thrust forces up to 49 N. The mounting assembly can be seen in Fig. 1(b). The assembly allowed the test rig to be rotated in the azimuthal direction, as indicated by the blue arrow.

The load cell was powered by a *Dewesoft SIRIUSiwe STG-M* unit, which also served as a data acquisition unit. To compensate for changes in static loading of the load cell, the ensemble was calibrated using a spring balance at every change in rotor axial spacing. The mean thrust was calculated from the mean value of the load cell signal over the duration of each recording, and the location of the highest peak in the PSD of the load cell signal was used to verify the motors' shaft frequency estimation from acoustic data, described further below.

Preliminary tests concluded that all blade counts could reach at least 8 N of thrust, hence all configurations were tested at 8 N (high thrust) and 4 N (low thrust). Most results are presented for 8 N only for the sake of brevity, as these are generally representative of the behaviour observed at 4 N as well.
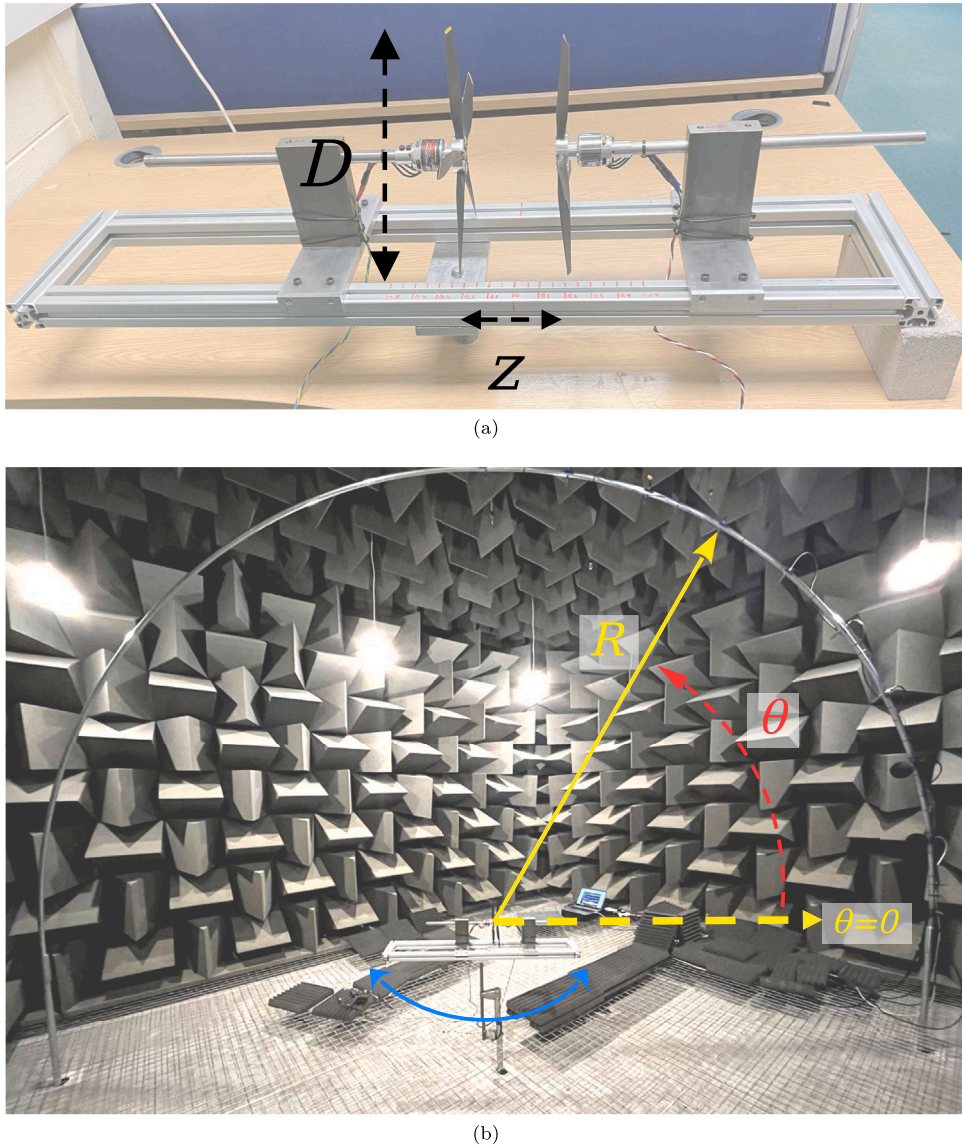
---

2 Information available at https://acoustictesting.salford.ac.uk/acoustic-laboratories/anechoic-chamber/.

(a)

(b)

Fig. 1. Custom-made contra-rotating propeller rig: (a) with propeller diameter *D* and axial separation *z* indicated; (b) with microphone array positioned inside the anechoic chamber, and emission angle θ and radius *R* indicated. The emission angle $\theta = 0°$ denotes the downstream direction, and $\theta = 180°$ denotes the upstream direction. (For interpretation of the references to colour in this figure legend, the reader is referred to the web version of this article.)

2.2. Data acquisition system

Acoustic pressure data were recorded by a semicircular microphone array arc made from aluminium poles, which were attached to the floor of the anechoic chamber. The microphones were installed at a radius $R = 2.5$ m (approximately $9D$), and emission angles between $\theta = 0°$ (on-axis, downstream) to $90°$, in $10°$ steps, totalling 10 microphones in the arc. This is illustrated in Fig. 1(b).

The microphones were fitted through $1/2$ in. holes in the frame, and were pointing directly towards the centre of the rig. Seven free-field *Brüel & Kjær 4966-H-041* microphones were used, combined with three *01dB MCE212* free-field microphone capsules connected to *GRAS 26CA* preamplifiers. As some measurements were performed with the microphones exposed to the flow downstream of the propellers, the three lower microphones were equipped with wind shields.

All ten microphones were connected to two *Dewesoft SIRIUSi* 8-channel units, set to a sampling rate $f_s = 50$ kHz. The *Dewesoft SIRIUSiwe STG-M* unit was connected to the load cell and set up with a sampling rate of $f_{s2} = 12.5$ kHz. The two *SIRIUSi* units were connected with the *SIRIUSiwe STG-M* via a *Dewesoft ECAT Sync Junction*, so all microphone and load cell measurement were synchronised by default. Measurements were carried out for a 30 s duration, and data was stored on a laptop connected to the units. A real-time monitoring screen was set up in *DewesoftX* software to observe the thrust and acoustic signals on the laptop screen.
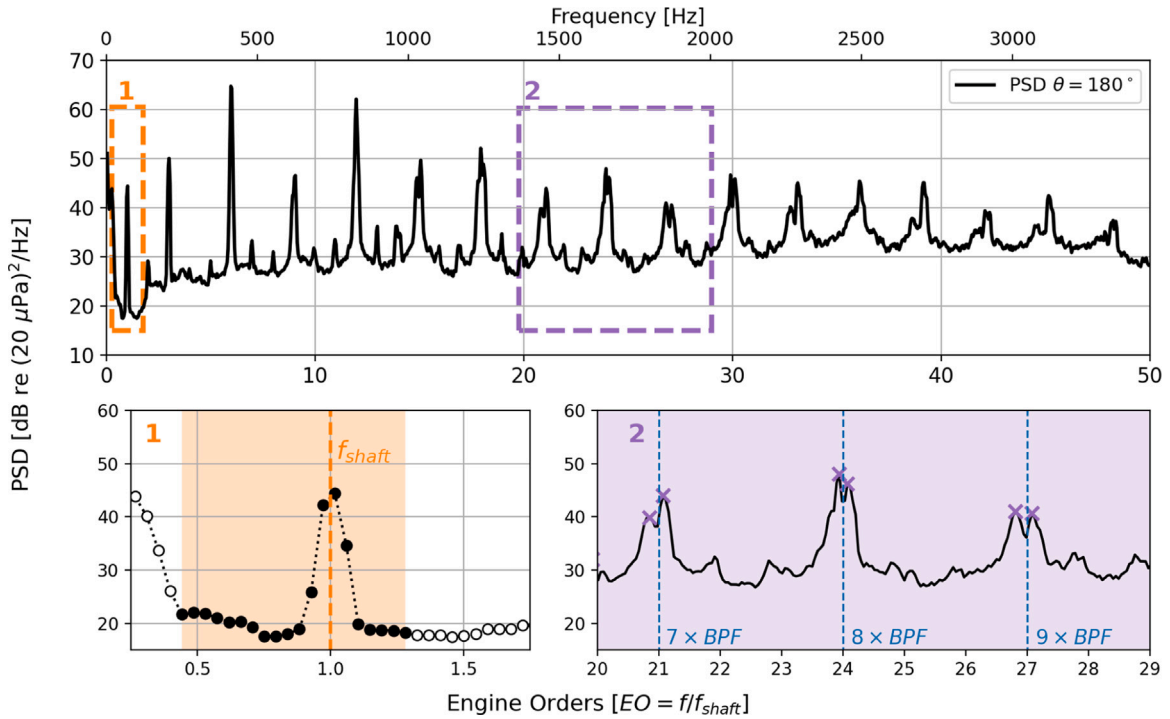
Fig. 2. Example PSD for 8 N thrust, 3 blades, axial spacing $z/D = 0.2$, and emission angle $\theta = 180°$. The frequency axis is shown as adimensional Engine Orders $EO = f/f_{shaft}$. Lower left: estimation of shaft frequency f_{shaft} by spectral centroid in the range [30, 90] Hz. Lower right: double peaks (crosses) occurring around higher BPF harmonics, evidencing the motors were rotating slightly asynchronously. (For interpretation of the references to colour in this figure legend, the reader is referred to the web version of this article.)

For each test configuration, both rotors were assembled with an equal number of blades and positioned at the desired axial separation distance z/D. Their rotational speeds were adjusted using the servo tester until the desired mean thrust value was observed from the load cell signal. Measurements were performed for a 30 s duration with the microphones downstream of the rig to obtain the noise at $\theta = 0°$ to $90°$. The rig was then rotated $180°$ in the azimuthal direction, and a new measurement was performed with the microphones positioned upstream to obtain the noise at $\theta = 90°$ to $180°$. This procedure was repeated for both 4 and 8 N thrust, and for all combinations of blade numbers and axial spacing.

Additionally, a few recordings were made with no blades attached to either propeller hub to estimate the motor-only noise. The speed controllers were adjusted to a typical rotational speed achieved during the previous tests, and the motor noise was recorded for 30 s. One motor-only measurement at $f_{shaft} = 66.2$ Hz is used for comparison with the other aeroacoustic measurements. It should be noted that motor noise likely depends on motor torque as well as rotational speed, and therefore the actual contribution of motor noise to the acoustic measurements might differ from the no-load results presented here.

2.3. Post-processing and data analysis

The recorded signals were processed in Python programming language, using modules from the SciPy scientific computing library [22]. The acoustic pressure Power Spectral Densities (PSDs) were calculated using Welch's method with a DFT size of 2^{14} samples, a Hann window function, and 50% overlap, resulting in approximately 180 averages and a frequency resolution of 3.1 Hz. The resulting power spectra were analysed in the band between $f_{lower} = 150$ Hz and $f_{upper} = 10$ kHz. The lower frequency limit was chosen to ensure fully anechoic behaviour in the test chamber, whereas the upper frequency limit was determined to avoid high frequency tonal artefacts presumed to be electric motor noise [18].

A typical PSD, in dB re $(20\ \mu Pa)^2/$ Hz, is shown in Fig. 2 for 8 N thrust, 3 blades, axial spacing $z/D = 0.2$, and emission angle $\theta = 180°$. The frequency axis is shown as adimensional Engine Orders $EO = f/f_{shaft}$. It was determined through visual inspection of the acoustic PSDs that the motors' shaft frequencies were the only peaks present between 30 Hz and 90 Hz in all cases. For each measurement, the shaft frequency f_{shaft} was estimated by calculating the spectral centroid of all channels' PSDs within this frequency range, shown by the shaded region in the lower left corner of Fig. 2, and taking the average of the estimated centroids across all channels. These estimates for f_{shaft} agreed well with the location of the higher BPF harmonics in the PSD, and with the main peak in the PSD of the load cell signal, as described above.

Despite both motors receiving the same control signal from the servo tester, small differences in the motor construction and propeller assembly led them to rotate at slightly different rates. This is evidenced by the double peaks that occur at higher BPF

harmonics in some cases, as shown in the lower right side of Fig. 2. An analysis of these peaks' locations yielded an estimated frequency difference of less than 2% between the two motors' rotational frequencies.

The broadband and tonal components were extracted from the raw PSD within the above mentioned frequency range. The broadband component of the PSD was estimated by applying a moving-median filter of 100 Hz bandwidth to the raw frequency spectra [8,9,23]. The moving-median filter estimates the broadband PSD at each frequency by calculating the median value of the original PSD over a 100 Hz-wide window centred at the desired frequency, ignoring a small number of high-amplitude outliers within the window such as tonal peaks. This "tone-deletion" method has been found satisfactory to estimate the broadband spectrum underneath tonal peaks as long as the median window bandwidth is wider than the frequency width of each tone, but smaller than the separation between two tones [24]. The overall Sound Pressure Level (OASPL) and the broadband SPL are obtained by integrating the original and the broadband PSDs over the frequency band $[f_{\text{lower}}, f_{\text{upper}}]$, and are reported in decibels relative to $p_{\text{ref}} = 20\ \mu\text{Pa}$ as

$$SPL(\theta) = 10 \log_{10}\left(\frac{\int_{f_{\text{lower}}}^{f_{\text{upper}}} S_{pp}(\theta, f)\,\mathrm{d}f}{(p_{\text{ref}})^2}\right). \tag{1}$$

The tonal component was calculated by searching for peaks in the spectrum at least 3 dB above the broadband component, determining the peak width from the intersection of the raw PSD with the broadband PSD, and subtracting the broadband noise contribution from the PSD values within the peak width. The tonal SPL is then calculated by integrating the contribution of all peaks in the original PSD within the peak's frequency width, as per Eq. (1) [25].

2.4. Sound Power Level PWL calculation

The above mentioned methods allow obtaining the SPLs for overall, tonal, and broadband components at each direction over the polar arc $\theta = 0°$ to $180°$. However, levels assessed at one direction might not be representative of the acoustic radiation at other angles, and a more global metric for the radiated sound level is required.

One such metric is the Sound Power Level, denoted PWL, characterising the sound power radiated by the acoustic source to the entire domain surrounding it. Assuming the acoustic radiation is symmetric around the axis $\theta = 0°$, the sound power P (in Watts) can be obtained by integrating the Power Spectral Densities over all emission angles as [26]

$$P = 2\pi \int_0^\pi \frac{S_{pp}(\theta)}{\rho c} R^2 \sin(\theta)\,\mathrm{d}\theta, \tag{2}$$

whereas the Sound Power Level PWL$= 10 \log_{10}(P/P_{\text{ref}})$ expresses this quantity in decibels relative to $P_{\text{ref}} = 10^{-12}$ W.

3. Aeroacoustic results

3.1. Acoustic spectra and SPLs at $\theta = 180°$

Fig. 3 shows a typical example of the Power Spectral Densities, in dB re $(20\ \mu\text{Pa})^2$/Hz, obtained in this experiment for a single emission angle in the rear arc of the propeller, at $\theta = 180°$, for axial spacings $z/D = 0.1, 0.3, 0.6,$ and 1.0 and mean thrust 8 N. This angle represents maximum emission for tonal interaction noise, while avoiding flow contamination present at $\theta = 0°$. The propellers were set up with three blades, and operated at 8 N mean thrust. The BPF harmonics are indicated by solid red circles, whereas other tones – such as f_{shaft} harmonics – are indicated by empty circles. The area under each tone is shaded in light red to help visualisation, and the frequency bandwidth of analysis $[f_{\text{lower}}, f_{\text{upper}}]$ is shaded light grey. The SPLs for tonal noise (including BPF and non-BPF tones), broadband noise, and overall (tonal plus broadband) noise are annotated on the lower left corner of each subplot.

In addition, the noise recorded from running the motors with no blades installed at $f_{\text{shaft}} = 66.2$ Hz (a frequency representative of the higher range of rotational frequencies analysed — see Table 2) is shown with a thin dotted line. The motor-only noise is below the aerodynamically-generated noise at all axial spacings and frequencies at 8 N thrust, and seldom protudes above aerodynamic noise for 4 N thrust. Therefore, it is not expected to interfere with the analysis and conclusions presented here.

The typical features of closely-spaced contra-rotating propeller noise, as previously discussed, can be seen in Fig. 3. In all cases, tonal noise dominates the spectrum between 150 Hz and approximately 4 kHz, whereas higher frequencies contain mostly broadband noise. Some shaft frequency tones are visible, indicated by the empty circles, possibly due to small imbalances between the propeller blades, but these are generally of much lower magnitude than the BPF harmonics indicated by the full circles. Due to slight differences in the rotational frequencies of the propellers, some BPF tones exhibit double peaks, indicated by overlapping full markers and detailed in Fig. 2.

High-amplitude interaction tones are visible in Fig. 3 at the shortest axial spacing $z/D = 0.1$ for even-order BPF harmonics ($2\times$BPF ≈ 400 Hz, $4\times$BPF ≈ 800 Hz, etc.), likely caused by potential field interaction. While the odd-order BPF harmonics do not exceed 50 dB re $(20\ \mu\text{Pa})^2$/Hz at this spacing, the interaction tones are up to 20 dB higher. The low-frequency tones (e.g. $1\times$BPF, $2\times$BPF) have a narrow base, indicating little or no nondeterministic narrowband noise. This configuration has the highest tonal noise SPL of all four shown here, at 80.8 dB SPL. At 68.7 decibels, the broadband noise SPL is lowest at this axial spacing, 12 dB below the tonal SPL. The OASPL is the highest at this axial spacing, at 81.1 dB.
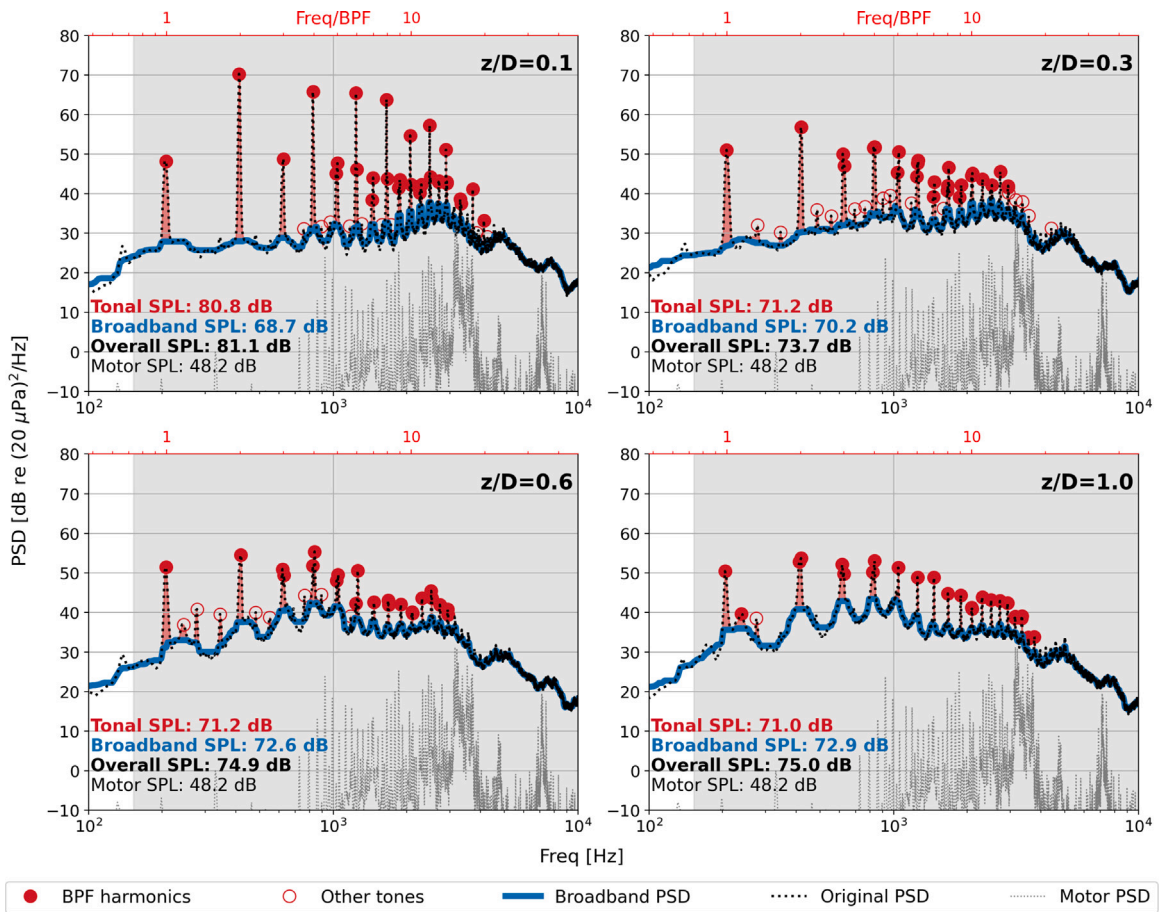
Fig. 3. Power Spectral Densities for a single observer at $\theta = 180°$, showing the original PSD (black dotted line), broadband PSD (solid blue line), BPF harmonics (solid red circles) and other tones (empty red circles). The noise from the motors only is shown in thin, grey dotted line, and the frequency range of analysis [150 Hz, 10 kHz] is shaded light grey. The propellers were operating at 8 N mean thrust and three blades, at normalised axial spacings $z/D = 0.1$, 0.3, 0.6, and 1.0. (For interpretation of the references to colour in this figure legend, the reader is referred to the web version of this article.)

As the axial spacing increases, the even-order BPF harmonics showing potential field interaction tones quickly decay in amplitude. The tonal noise SPL has decayed almost 10 dB at axial spacing $z/D = 0.3$, on the top right side of Fig. 3, and the difference between even- and odd-order BPF tones' magnitudes is now less than 10 decibels. A slight increase in broadband noise at mid frequencies, near 900 Hz, can be observed. At this axial spacing, both tonal SPL (71.2 dB) and broadband SPL (70.2 dB) are within 1 dB of each other, and contribute almost equally to the OASPL. This axial spacing also shows the lowest OASPL, at 73.7 dB.

On the lower left corner of Fig. 3, at $z/D = 0.6$, no clear distinction is visible between even- and odd-order BPF tones' amplitudes, indicating a significant reduction in rotor–rotor potential field interaction. The lower BPF harmonics now exhibit a wider base, indicating some nondeterministic narrowband noise, and the broadband PSD has increased by about 10 dB around 800 Hz compared to that for $z/D = 0.1$. The OASPL for this configuration is slightly dominated by broadband noise, with a 1.4 dB difference between tonal SPL (71.2 dB) and broadband SPL (72.6 dB).

Finally, the lower right corner of Fig. 3 shows the PSD for the largest axial spacing $z/D = 1.0$. Although the lower BPF harmonics clearly exhibit a wider base (and thus more nondeterministic narrowband noise), this configuration exhibits only a small increase in broadband noise compared to $z/D = 0.6$, with a 1.9 dB difference between tonal SPL (71.0 dB) and broadband SPL (72.9 dB).

Results for 4 N mean thrust showed slightly lower levels, but followed the same trends described above for 8 N thrust.

3.2. Changes in SPL with axial spacing and number of blades

The trends in SPLs for changes in axial spacings and blade numbers are shown in Fig. 4. Trends are shown for three emission angles: $\theta = 180°$ in Fig. 4(a), $\theta = 90°$ in Fig. 4(b), and $\theta = 40°$ in Fig. 4(c). The axial spacing of minimum OASPL is indicated by a red circle in each subplot.

Fig. 4 allows comparing SPL trends over different blade numbers and axial spacings. For emission angle $\theta = 180°$ (Fig. 4(a)), all blade numbers follow the trends previously described: tonal noise dominates the OASPL at very short axial spacings due to potential
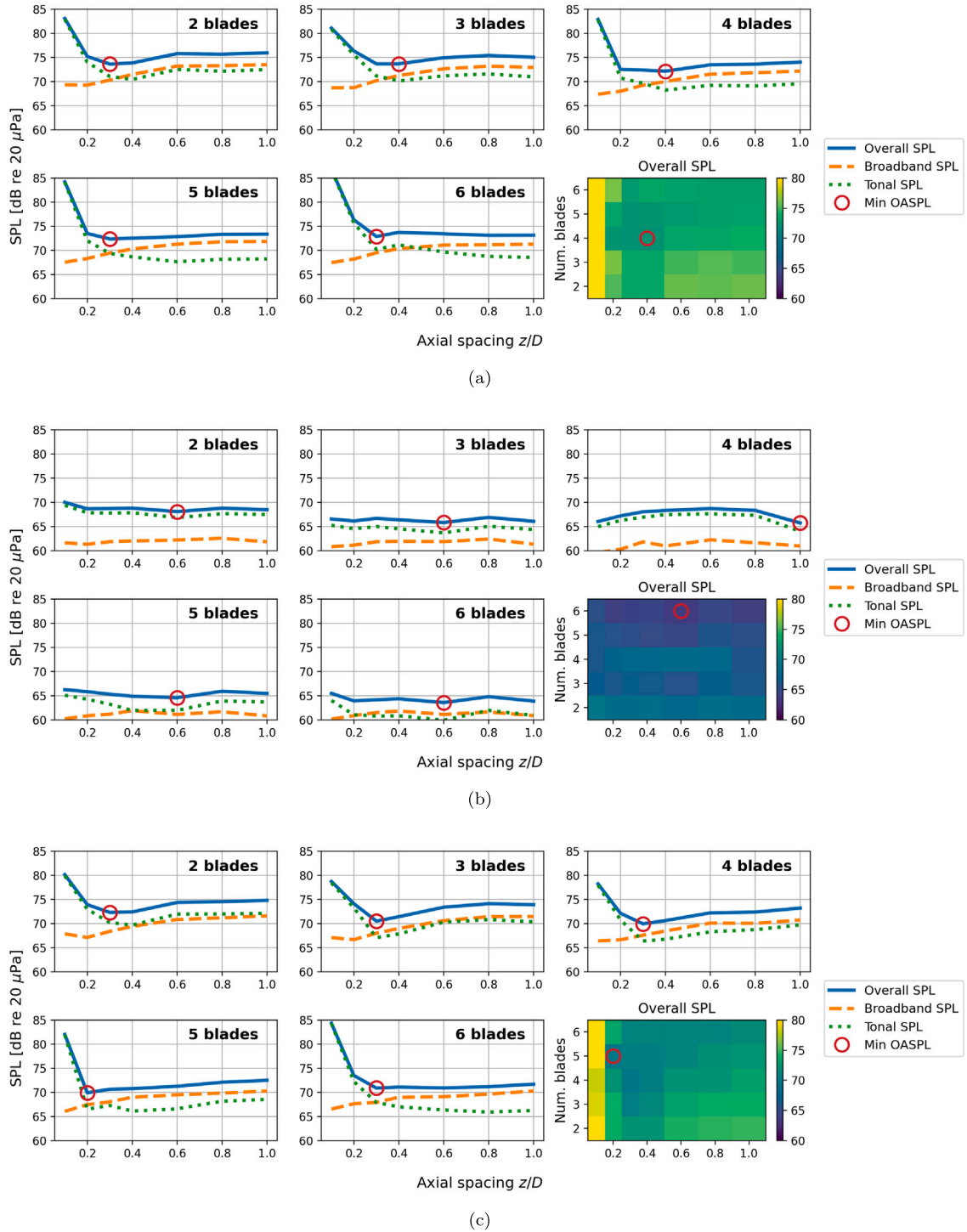
Fig. 4. Overall (solid blue), broadband (dashed orange), and tonal (dotted green) Sound Pressure Levels versus axial spacing z/D for observers at different emission angles θ, for multiple number of blades in the rotors and 8 N thrust: (a) θ = 180°; (b) θ = 90°; (c) θ = 40°. The minimum OASPL is indicated by a red circle in each subplot. (For interpretation of the references to colour in this figure legend, the reader is referred to the web version of this article.)
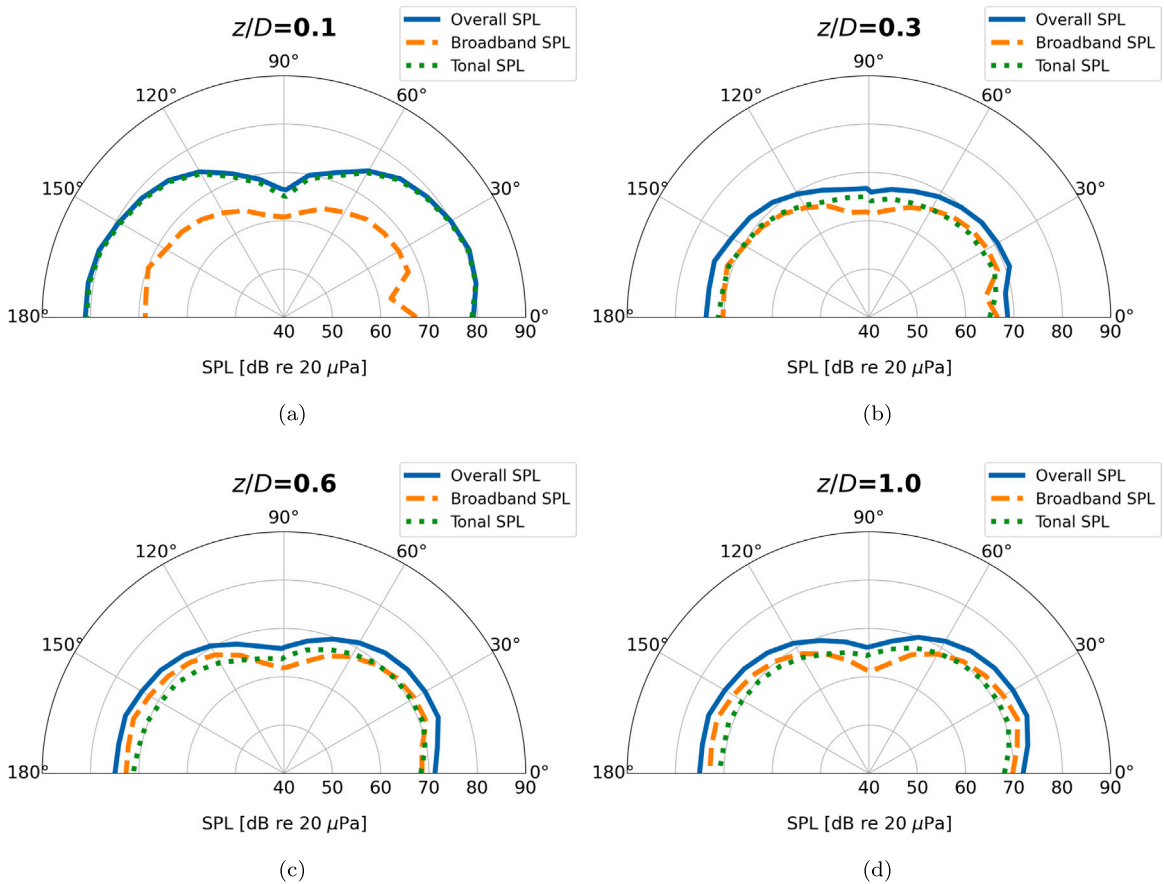
Fig. 5. Far-field directivities of overall SPL (solid blue), broadband SPL (dashed orange), and tonal SPL (dash-dotted green). The propellers were operating at 8 N mean thrust, and assembled with 3 blades and varying axial spacing: (a) $z/D = 0.1$; (b) $z/D = 0.3$; (c) $z/D = 0.6$; (d) $z/D = 1.0$. (For interpretation of the references to colour in this figure legend, the reader is referred to the web version of this article.)

field interaction, and broadband noise is at a minimum. Broadband noise is seen to increase steadily as axial spacing increases due to higher turbulent wake interaction, while tonal noise reaches a minimum and then increases slightly for lower blade counts, likely due to tip vortex interaction. In all cases, a minimum OASPL can be identified at the axial separation where broadband and tonal noise show comparable magnitudes, indicated by the red circle.

The general trends in OASPL become more apparent by plotting OASPL versus blade count and axial spacing, shown as a pseudocolor map in the lower right corner of Fig. 4(a). At short axial spacings, the OASPL increases with blade count, reflecting the increased tonal noise due to stronger interaction between propellers with many blades. On the other hand, the OASPL decreases with increasing blade count at large axial spacing, reflecting a decrease in both broadband and tonal SPLs. This reduction in SPL with increasing blade number might be related to the reduced blade tip Mach number required to achieve the same thrust with more blades. A minimum OASPL configuration is obtained with 4 blades and $z/D = 0.4$, although other configurations with axial spacings between $z/D = 0.3$–0.4 and 4–5 blades per rotor achieve similarly reduced OASPL for this emission angle.

At $\theta = 90°$ emission angle, shown in Fig. 4(b), a different set of trends emerge: broadband noise remains consistently low at all blade counts, while tonal noise – and consequently, OASPL – generally decreases with increasing number of blades. The exception is the contra-rotating configuration with 4 blades per rotor, which shows higher tonal noise levels than either 3 or 5 blades. No clear dependence of any SPL metric on axial spacing is observed. Consequently, there is no clear range of configurations that yield significantly reduced OASPL at this emission angle.

Finally, Fig. 4(c) shows the results at $\theta = 40°$, an emission angle representative of a typical observer interacting with a UAV. The trends seen here follow those discussed for $\theta = 180°$ and shown in Fig. 4(a), with tonal noise increasing with increasing blade counts at short axial spacings, and decreasing with increasing blade counts at large axial spacings. Broadband noise increases with axial spacing, but does not change significantly with blade count. The minimum OASPL configuration for this observer is 5 blades per rotor and axial separation $z/D = 0.2$, but configurations with axial spacings between $z/D = 0.3$–0.4 and 4–5 blades per rotor can once again achieve similarly reduced OASPL.

3.3. Noise direcivity

The unclear behaviour observed at $\theta = 90°$ can be further explained by the directivity plots of each SPL metric of the contra-rotating propellers. Fig. 5 below shows the directivities for the same configuration discussed in Fig. 3: 3 blades, 8 N thrust, over multiple axial spacings. The OASPL is shown as solid blue lines, the broadband SPL as dashed orange lines, and the tonal SPL as dotted green lines.

Fig. 5 shows that both broadband and tonal noise have a directivity function close to that of a point dipole aligned with the $\theta = 0°$ axis, as expected for loading noise sources. As the axial separation z/D increases, broadband noise continues to present a dipole radiation pattern, whereas tonal noise changes and does not display a strong null at $\theta = 90°$ any longer, indicating potential contribution from steady loading noise. This noise source is primarily driven by convective amplification instead of surface pressure fluctuations, hence its directivity is not dipole-like [3].

The trends previously established for $\theta = 180°$ and $\theta = 40°$ emission angles appear to hold for all out-of-plane emission angles over the range of axial spacings shown in Fig. 5. The exception is for angles near the propeller plane, between $60°$ and $120°$, where less well-defined changes in noise levels are observed due to the null in the directivity function. It is expected that trends observed at other emission angles will not correlate well to changes observed in this region.

3.4. Sound Power Level PWL analysis

The previous results indicate that optimising a contra-rotating propeller system for reduced noise at one emission angle might not provide similar reductions at other angles. This section investigates whether the Sound Power Level PWL provides a more robust optimisation metric by considering the sound radiated in all directions simultaneously.

The Sound Power Level PWL (in dB ref 10^{-12} W) was calculated using Eq. (2) for the Overall, broadband and tonal PSDs over all blade numbers and axial spacings. The results for 4 N thrust are shown in Fig. 6(a) below, and for 8 N thrust are shown in Fig. 6(b).

The trends in PWL seen in Fig. 6 are similar to those observed for on-axis SPLs in Fig. 4. Large overall levels are apparent for very short axial distances, while at larger distances a general decrease in level is apparent for larger blade counts. As before, a region of minimum PWL is seen at distances near $z/D = 0.2$–0.4 and higher blade numbers, with a global minimum for 4 blades and $z/D = 0.4$ at 4 N thrust, and 5 blades and $z/D = 0.3$ at 8 N. These optimal low-noise configurations are similar to those obtained for minimum SPL at $\theta = 180°$ and $\theta = 40°$, showing that the PWL is a robust metric against nulls in the acoustic radiation.

Note that the axial spacing for minimum PWL is $z/D = 0.4$ for 4 out of 5 cases at 4 N thrust (Fig. 6(a)), whereas it is $z/D = 0.3$ for all 5 cases at 8 N thrust (Fig. 6(b)). This could indicate that contra-rotating propellers' acoustically optimal separation is dependent on other aerodynamic parameters such as blade pitch and/or helicoidal Mach number, but further research is required to verify this hypothesis [1,9].

4. Psychoacoustic analysis

In addition to the acoustic analysis described in the previous section, the noise signals acquired from the microphone array were exported as .WAV files and processed through *HEAD Acoustic ArtemiS Suite 12.0* software to calculate a series of Sound Quality Metrics. All SQMs time series were processed in Python by removing their first 0.5 s to avoid transient effects in the calculations, and determining their 5th percentiles (or 5% exceedance levels [13]) to represent the higher range of each SQM time history [7]. The 5th percentile is a widely accepted approach for summarising time-varying values of SQMs into a single value, and has been found to correlate well with the subjective evaluation of aircraft noise [27].

The model of Loudness (measured in sone) used for the analysis of the perception of sound level was DIN45631/A1, which is a standardisation of the Zwicker Loudness model. To account for the perceptual effect of spectral and temporal characteristics of the sounds evaluated, other SQMs were calculated: Fluctuation Strength (measured in vacil), Roughness (measured in asper), Impulsiveness (measured in Impulsiveness Units — IU), and Tonality (measured in Tonality Units — TU). Fluctuation Strength, Roughness, Impulsiveness and Tonality metrics were calculated using the hearing model developed by Sottek [28]. The Sottek's hearing model accounts for the signal processing chain present in the human auditory system, modelling the sound propagation through the outer and middle ear, and the frequency selectivity at the inner ear. The Tonality hearing model of Sottek, described in detail in the ECMA-74 standard [29], assesses perceived tonality as a function of the overall loudness tonal-to-noise ratio across all frequency bands. Further details about these SQMs can be found at Torija et al. [7].

4.1. Sound samples

The SQMs described above were calculated for the subset of sounds generated by the contra-rotating test rig with blade counts from 2 to 6, rotor–rotor axial spacings between $z/D = 0.1$ to 1.0, thrust settings of 4 and 8 N, and emission angles of $\theta = 90°$ and $\theta = 180°$. A subset of 36 sound samples was selected for a psychoacoustic experiment, where a series of participants were asked to provide a subjective rate of noise annoyance for each sound sample presented. The psychoacoustic experiment was designed to maximise the amount and quality of the data collected, while minimising listener fatigue [30]. For this reason, a compromise was made in the rotor–rotor axial spacing and blade count configurations investigated in the psychoacoustic experiment. The main criterion for selection was to include sound samples including rotor–rotor axial spacings with varying amplitude of interaction tones, and emission angles with maximum and minimum radiation of interaction tones. This selection was based on the findings of Torija
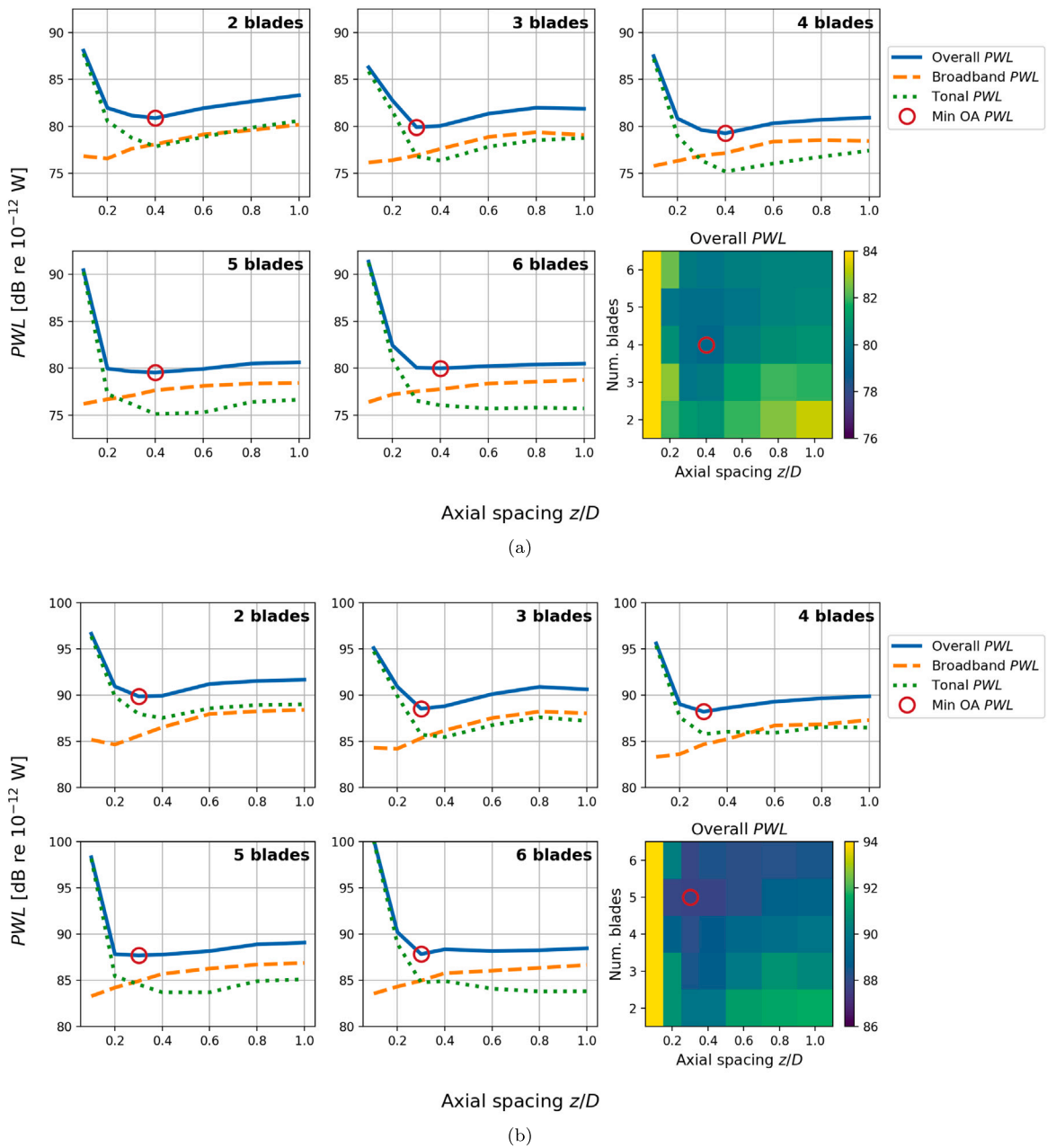
Fig. 6. Overall (solid blue), broadband (dashed orange), and tonal (dotted green) Sound Power Levels PWL versus axial spacing z/D for multiple number of blades and thrust: (a) 4 N mean thrust; (b) 8 N mean thrust (note different values on vertical axes). The axial spacing of minimum Overall PWL is indicated by a red circle in each plot. (For interpretation of the references to colour in this figure legend, the reader is referred to the web version of this article.)

et al. [7,15]. Configurations with 2, 4 and 6 blades were considered in the psychoacoustic experiment to cover the whole range of blade counts measured. Table 3 shows a summary of the different combinations of number of blades, thrust setting, rotor–rotor axial spacing and emission angle in the sound samples selected.

These sound samples were organised in 9 groups, each containing 5 sound samples: one "reference sound" and four test sounds. Each sound was 4 s in length. The sound levels of the test sounds ranged from $L_{Aeq,4s} = 55$ dBA to 85.6 dBA. The reference sound was carefully selected to not include any significant prominence in sound character and a sound level approximately at the centre of the range for test sounds. A sound with 2 blades, 8 N, $z/D = 0.2$ axial spacing, and 180° emission angle was selected as reference. The sound level of the reference sound was $L_{Aeq,4s} = 76.6$ dBA. This reference sound was carefully selected, as having an important impact on the subjective evaluation of the sound samples [31]. The criterion was to select a sound that did not have any dominant sound quality characteristics, such as tonality or amplitude modulation, and therefore with a more broadband-type character.

Table 3
Summary of sound samples used in the psychoacoustic experiment.

Sample number	Number of blades	Thrust	Axial spacing	Emission angle
1	2	4 N	0.1 z/D	180°
2	2	4 N	0.1 z/D	90°
3	2	4 N	0.3 z/D	180°
4	2	4 N	0.3 z/D	90°
5	2	4 N	1.0 z/D	180°
6	2	4 N	1.0 z/D	90°
7	2	8 N	0.1 z/D	180°
8	2	8 N	0.1 z/D	90°
9	2	8 N	0.3 z/D	180°
10	2	8 N	0.3 z/D	90°
11	2	8 N	1.0 z/D	180°
12	2	8 N	1.0 z/D	90°
13	4	4 N	0.1 z/D	180°
14	4	4 N	0.1 z/D	90°
15	4	4 N	0.3 z/D	180°
16	4	4 N	0.3 z/D	90°
17	4	4 N	1.0 z/D	180°
18	4	4 N	1.0 z/D	90°
19	4	8 N	0.1 z/D	180°
20	4	8 N	0.1 z/D	90°
21	4	8 N	0.3 z/D	180°
22	4	8 N	0.3 z/D	90°
23	4	8 N	1.0 z/D	180°
24	4	8 N	1.0 z/D	90°
25	6	4 N	0.1 z/D	180°
26	6	4 N	0.1 z/D	90°
27	6	4 N	0.3 z/D	180°
28	6	4 N	0.3 z/D	90°
29	6	4 N	1.0 z/D	180°
30	6	4 N	1.0 z/D	90°
31	6	8 N	0.1 z/D	180°
32	6	8 N	0.1 z/D	90°
33	6	8 N	0.3 z/D	180°
34	6	8 N	0.3 z/D	90°
35	6	8 N	1.0 z/D	180°
36	6	8 N	1.0 z/D	90°

4.2. Participants

A total of thirty one participants took part in the experiment: twenty three males (74%), seven females (23%) and one nonbinary person (3%). The number of participants taking part in the listening experiment is consistent with common practice found in literature [15,31]. Twenty one participants were 18–34 years old, and ten participants over 35 years old. Most participants (61%) had English as their native language, and 39% had other languages as native language (including Chinese, Malayalam, Spanish and Portuguese). Prior to starting the experiment, all participants were asked to self-certify their hearing ability. Only 10% of the participants self-identified as having a hearing impairment. It was decided to keep these subjects in the study, as the cases were mild tinnitus and a small loss of high-frequency hearing (above 8 kHz), and neither interfered with the participants' day-to-day life.

Before analysing the participants' responses, an outlier analysis was carried out. During this analysis, responses deviating more than 3 times the standard deviation of all the participants' responses for each sound sample were discarded. A total of 17 responses from 5 participants were discarded for the analysis, out of more than 1000 responses from 31 participants.

4.3. Experimental setup and procedure

Ethics approval was granted by the University of Salford's Ethics Committee (ID 6068) for the listening experiment method and data collection procedure. The grounds of this approval were granted based on the participants being treated correctly in terms of transparency of the experiment, that participant safety be of utmost importance (e.g. they will not be exposed to excessively loud sounds), and consent of the participant is explicitly obtained but could be revoked by the participant at any time without reason. Subject privacy was also of critical importance, with any sensitive information being collected and stored in line with the UK General Data Protection Regulation (UK GDPR).

The psychoacoustic experiment was carried out within the University of Salford Listening Room. This listening room is acoustically treated to reduce both reverberation and ambient sound levels, with the L_{Aeq} measured between 20–22 dBA.

The audio reproduction system consisted of a laptop with *Mathworks MATLAB* software, *MOTU 4Pre* audio interface, *Little Labs Monotor* headphone amplifier, and *beyerdynamic DT 1990 Pro* headphones. The headphones were an open-back design and provided minimal isolation from external sounds, so equipment used during the experiment (e.g., laptop) was positioned away from the
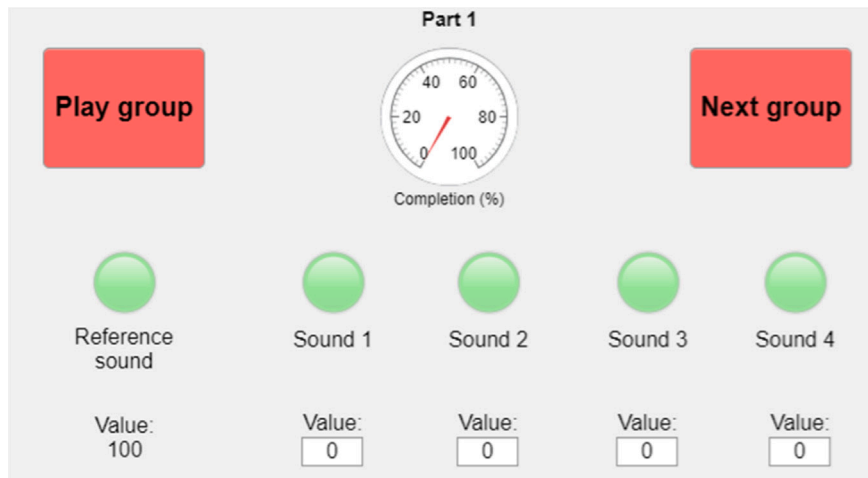
Fig. 7. User interface to report noise annoyance of test sounds.
Source: From Torija et al. [15].

participants and covered with acoustic foam. The contribution from ambient sounds within the listening room were concluded negligible during pilot sessions. Before the experiment took place, the sound samples used in the psychoacoustic experiment were calibrated to the "correct" sound level (L_{ASmax}) as measured in the anechoic chamber. The equipment used for the calibration of the audio files and listening experiment set-up included a *Brüel & Kjær Type 2250* Class 1 Sound Level Meter (SLM) and *Brüel & Kjær Type 4153* Artificial Ear. A calibration level within 0.5 dB of the L_{ASmax} value measured was considered suitably calibrated.

Following a procedure implemented in Torija et al. [15], the participants were asked to rate the annoyance of each of the test sounds within a group relative to a reference sound. Test sounds were randomly allocated to each of the 9 groups of sounds for evaluation. In each group the reference sound was given an annoyance rating of "100" and the participant was asked to rate the 4 remaining test sounds against this annoyance level. Using the user interface showed in Fig. 7, the participants reported the annoyance of each of the test sounds within a group. Once they completed the assessment of a given group, they moved to another group until the 9 groups of sounds were assessed.

5. Psychoacoustic results

Fig. 8 shows the variability in reported annoyance for each sound sample. There was great consistency in the participants' responses of noise annoyance for the 36 sound samples evaluated, with only a few outliers (e.g. sound sample S31). The average Coefficient of Variation (CoV) of noise annoyance responses for all 36 sound samples is 0.3 ± 0.1.

Figs. 9, 10, 11, 12 and 13 show the 5th percentile value of the SQMs Loudness, Tonality, Fluctuation Strength, Roughness and Impulsiveness as a function of rotor–rotor axial spacing, for different number of blades, thrust and emission angle. The 5th percentile are SQM values that are exceeded 5% of the time, and therefore minimise the influence in the analysis by other noise sources other than the sound source under investigation.

As shown in Fig. 9, at $\theta = 180°$, there is a clear reduction of Loudness as the contra-rotating rotors are moved further apart for all blade counts. This decrease in Loudness is more pronounced at 8 N. The lowest values of Loudness are observed at axial distances $z/D = 0.2$–0.4 at all cases, while for $z/D > 0.4$ there is a slight increase in Loudness. This confirms the findings of Torija et al. [7,15], where potential field interaction tones were found as the dominant noise source for closely spaced rotors and enhanced turbulence-propeller interaction noise was found as the dominant noise source for rotors spaced further apart. There are two important findings here: (1) the region of lowest Loudness has been found to be consistent for all the blade counts evaluated; (2) there is a decrease in Loudness from low to high blade counts at constant thrust. At $\theta = 90°$, the values of Loudness seem to be independent from the rotor–rotor axial spacing, but a decrease in Loudness from low to high blade counts is also observed.

As shown in Fig. 10, an important reduction of Tonality with the increase of the rotor–rotor axial spacing is observed at $\theta = 180°$ for all blade counts evaluated. For both 4 and 8 N, the lowest values of Tonality are consistently found at axial distances $z/D \geq 0.3$. In this case, there seems to be an increase in Tonality with the increase in blade count. This might be due to the displacement of the BPF (and its harmonics) towards high frequencies as the blade count increases, leading to an increase of tonal noise in frequency regions where the Tonality metric is more sensitive. Alternatively, Tonality might be increasing due to stronger potential field interactions for rotors with higher blade counts. At $\theta = 90°$, the values of Tonality seem to be independent from the rotor–rotor axial spacing, and there is not a clear pattern in the values of Tonality with changes in the blade count. There is a significantly high value of Tonality for the configuration with 4 blades at 8 N. This seems to be consistent with Fig. 4(b), where an increase in tonal noise compared to other blade counts is observed. A combination of prominence of tonal noise over broadband noise and
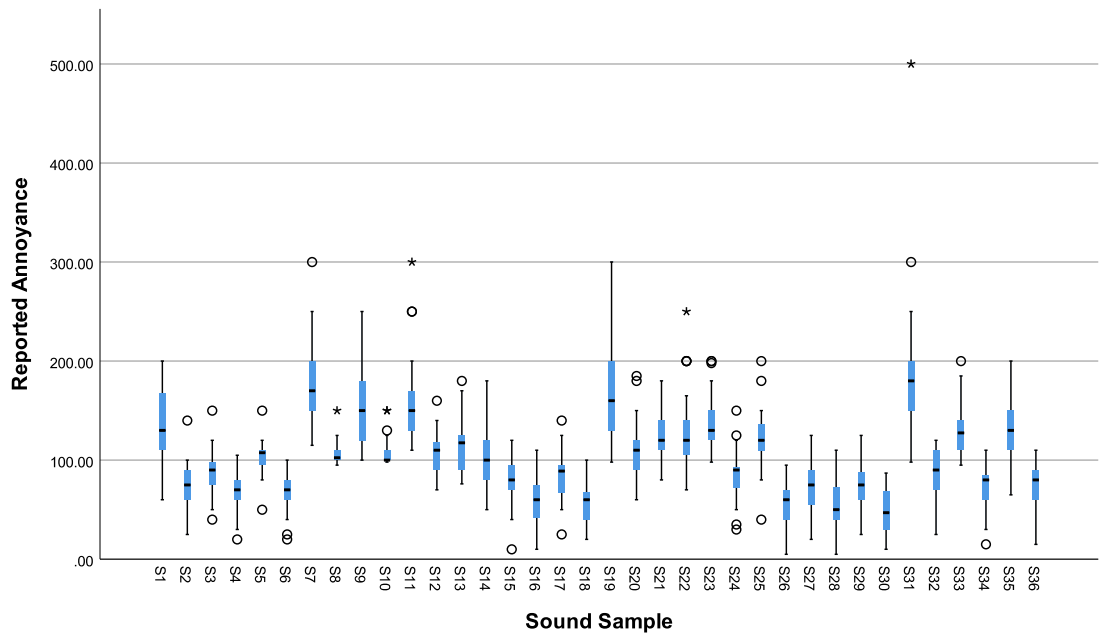
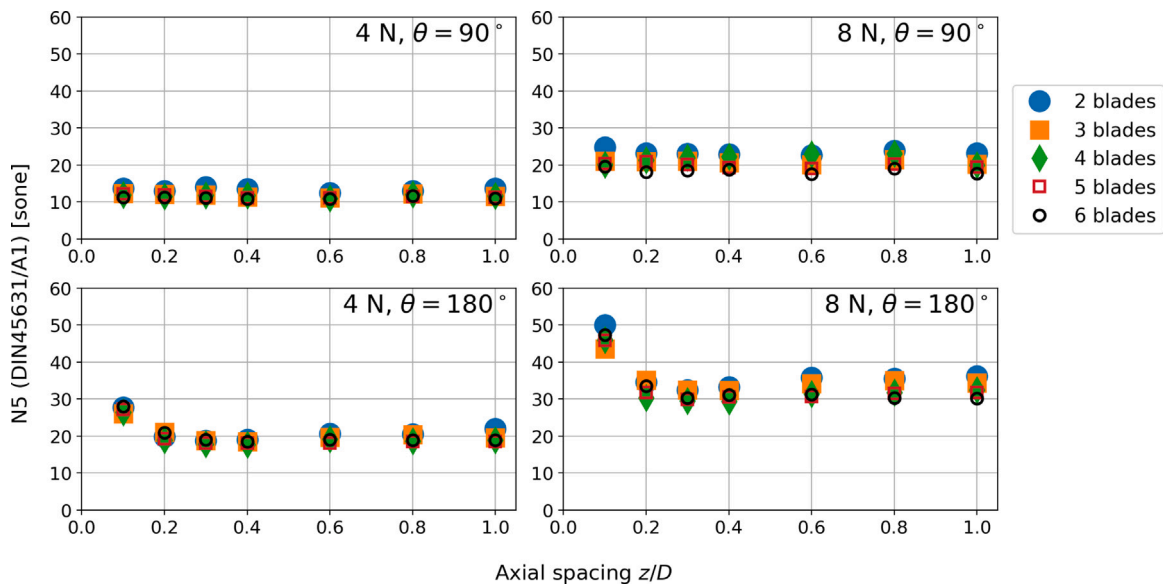Fig. 8. Variability of participants' responses of noise annoyance for each sound sample.

Fig. 9. 5th percentile value of the Loudness metric as a function of rotor–rotor axial spacing, for different number of blades, thrust setting (4 N on the left side, and 8 N on the right side) and emission angle θ (90° on the top side, and 180° on the bottom side).

displacement of the BPF (and its harmonics) towards the high frequency region might be a possible explanation for this. However, further research is needed to confirm the cause of this increase in tonal noise for this particular configuration.

Observing Fig. 11, at $\theta = 180°$ and 4 N, there seems to be a tendency of the Fluctuation Strength values to decrease with an increase of the rotor–rotor axial distance (with only two outliers of the 4 and 6 blade configurations at z/D = 0.2 and 0.4 respectively) At 8 N, the reduction of Fluctuation Strength with the increase of the axial spacing is only observed for the 2 blades configurations, while for the other blade counts the value of Fluctuation Strength does not seem to depend on the axial spacing. Torija et al. [7,15] suggested Fluctuation Strength to be related to amplitude modulation caused by interaction (or "beating") effects between potential field interaction tones, and found a decrease in Fluctuation Strength values with an increase of axial spacings in a contra-rotating test rig with two-bladed rotors. Such amplitude modulation phenomenon (with low modulation frequency) seems to be less dependent
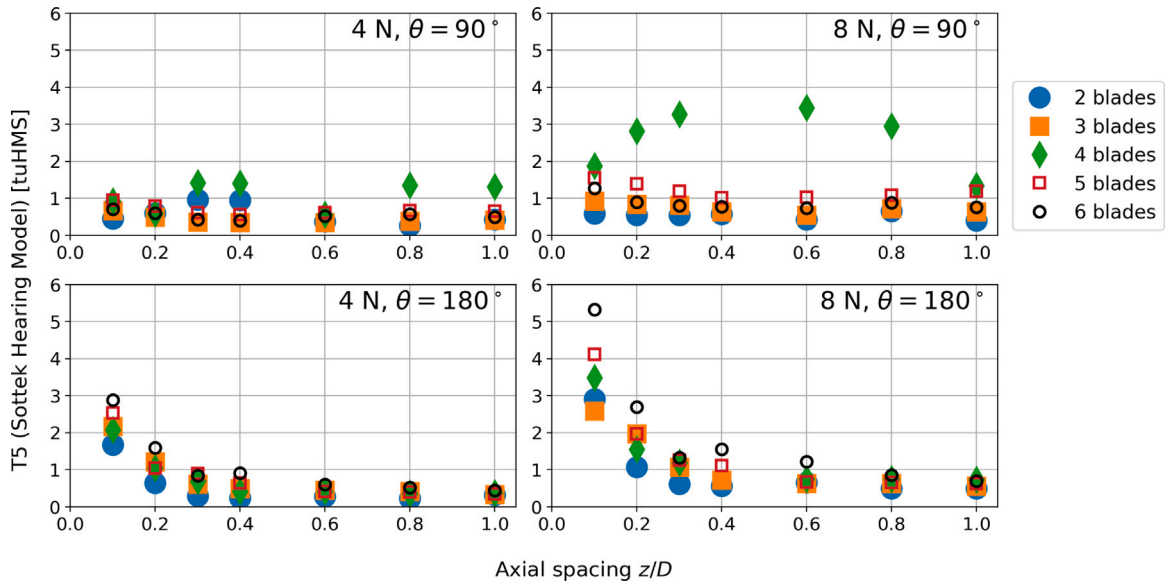
Fig. 10. 5th percentile value of the Tonality metric as a function of rotor–rotor axial spacing, for different number of blades, thrust setting (4 N on the left side, and 8 N on the right side) and emission angle θ (90° on the top side, and 180° on the bottom side).
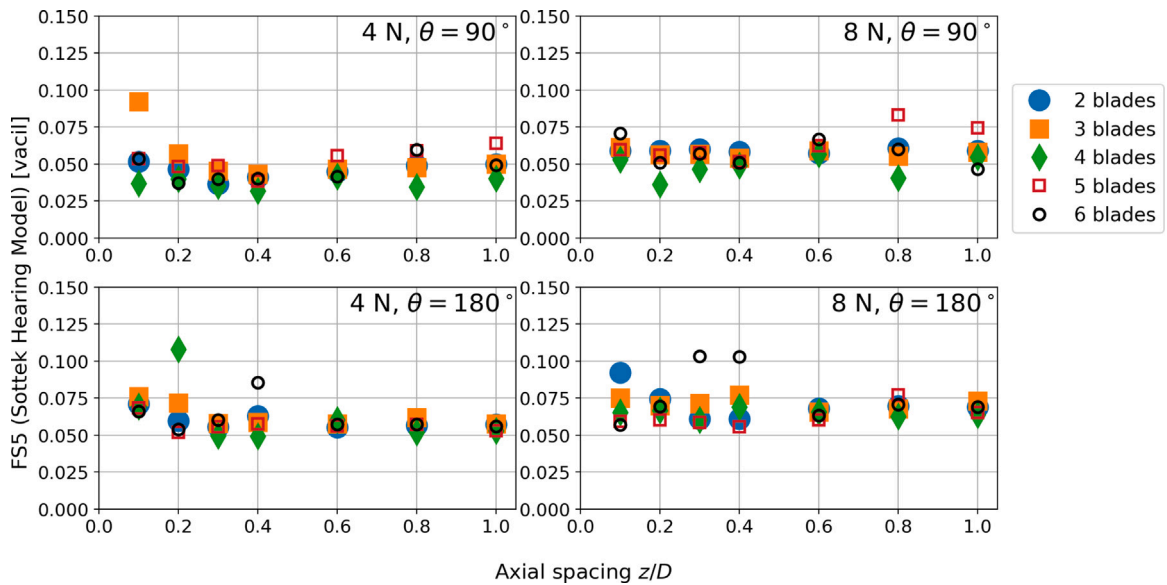

Fig. 11. 5th percentile value of the Fluctuation Strength metric as a function of rotor–rotor axial spacing, for different number of blades, thrust setting (4 N on the left side, and 8 N on the right side) and emission angle θ (90° on the top side, and 180° on the bottom side).

on the rotor–rotor axial spacing for high blade counts at 8 N. At $\theta = 90°$ and 4 N, a region of generally reduced Fluctuation Strength values is observed around z/D = 0.4. At 8 N, no clear tendency is observed.

In Fig. 12, it can be observed that Roughness values decrease with an increase in rotor–rotor axial spacing for all blade counts at $\theta = 180°$. Roughness quantifies the loudness modulations with high modulation frequencies (i.e., too high to be discerned separately). As for Fluctuation Strength, Roughness seems to decrease as the interaction effects between rotors lessen with the increase of axial spacing. Roughness is also observed to decrease in configurations with higher blade counts. A possible explanation could be the increase in the modulation frequency for higher blade counts, moving away from the modulation frequency region leading to maximum values of Roughness [27]. At $\theta = 90°$, there is a general tendency of Roughness to decrease with an increase in blade count, but Roughness values seem to be less dependent on rotor–rotor axial spacing.

As shown in Fig. 13, at $\theta = 180°$, Impulsiveness clearly increases with the increase of the rotor–rotor axial spacing. As discussed by Torija et al. [7], an increase in highly impulsive noise caused by enhanced turbulence-propeller interactions is observed when
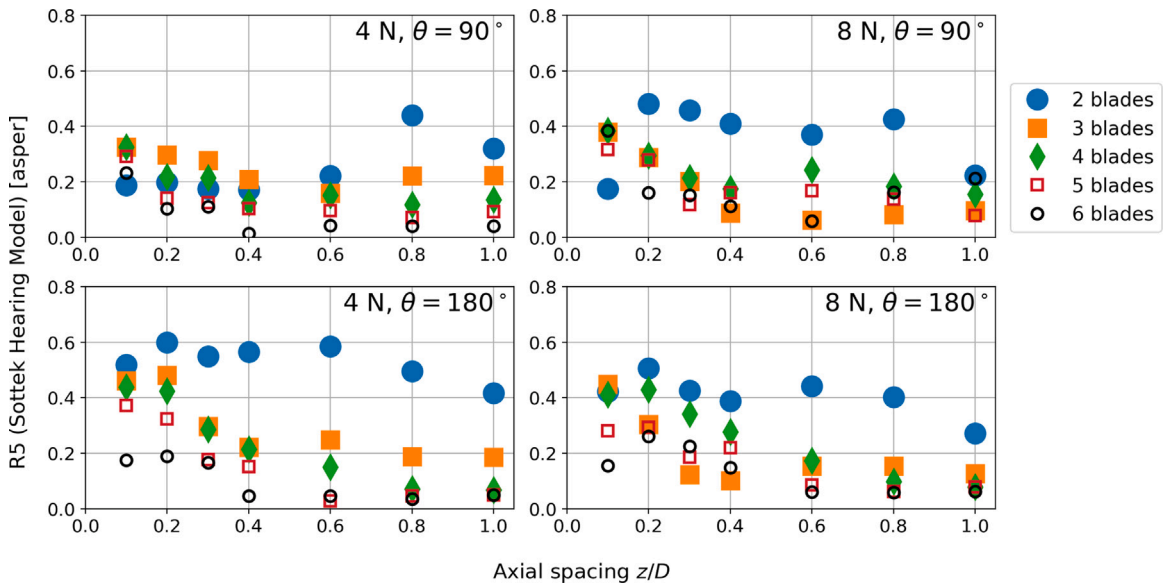
Fig. 12. 5th percentile value of the Roughness metric as a function of rotor–rotor axial spacing, for different number of blades, thrust setting (4 N on the left side, and 8 N on the right side) and emission angle θ (90° on the top side, and 180° on the bottom side).
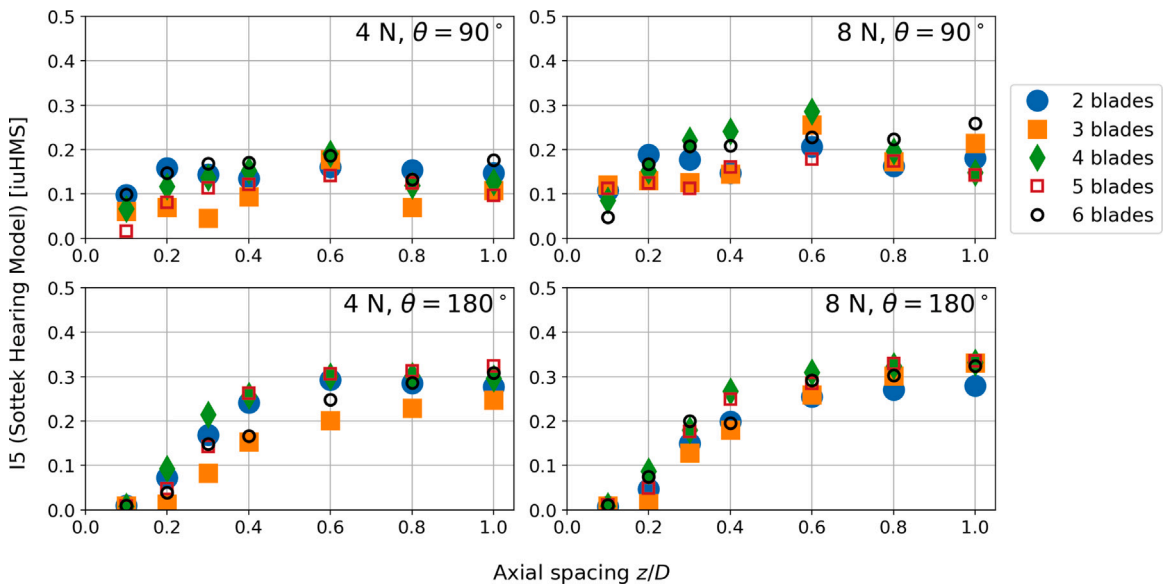

Fig. 13. 5th percentile value of the Impulsiveness metric as a function of rotor–rotor axial spacing, for different number of blades, thrust setting (4 N on the left side, and 8 N on the right side) and emission angle θ (90° on the top side, and 180° on the bottom side).

contra-rotating rotors move apart from each other, leading to an increase in Impulsiveness. There is no clear pattern observed in the values of Impulsiveness with changes in the blade count. At θ = 90°, only a slight increase in Impulsiveness with an increase of axial spacing is observed for the 8 N cases.

Fig. 14 shows the annoyance level reported by the participants of the psychoacoustic experiment as a function of rotor–rotor axial spacing, for different number of blades, thrust setting and emission angle. At emission angle θ = 180° (left side of Fig. 14), configurations with 4 and 6 blades are reported as less annoying than configurations with 2 blades for both thrust settings. A similar trend of annoyance level vs. rotor–rotor axial spacing has been found for the three blade counts and two thrust settings evaluated: a significant decrease in the annoyance levels reported is observed from an axial spacing of 0.1 to 0.3; a slight increase in annoyance levels is then observed at 1.0 axial spacing, compared to an axial spacing of 0.3. This is consistent with results presented here and in previous literature [15]. At 4 N, the decrease in annoyance levels from 0.1 to 0.3 axial spacing is very similar for the three blade counts (30% for 4 blades and 38% for 6 blades); at 8 N, the decrease in annoyance levels from 0.1 to 0.3 axial spacing is notably
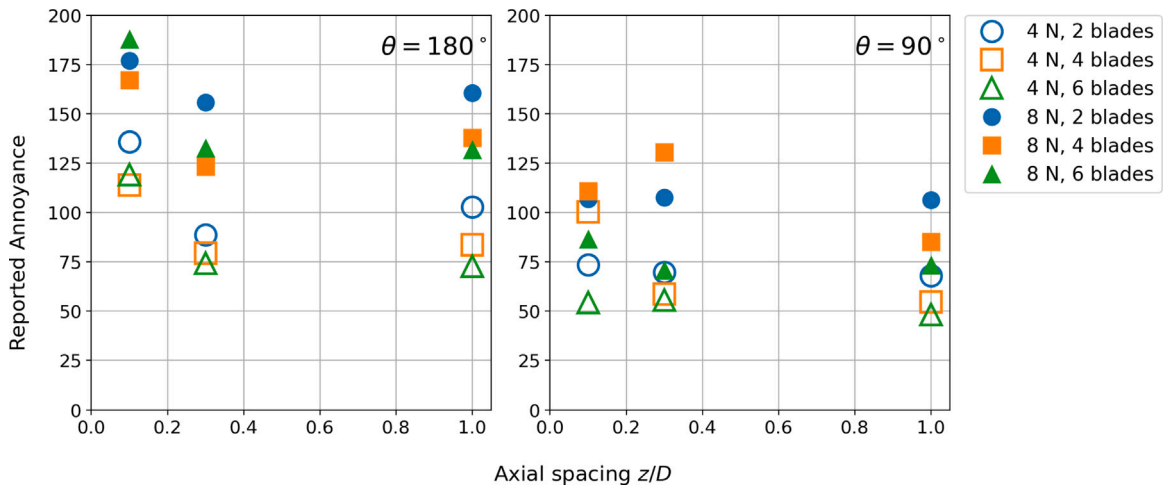
Fig. 14. Reported annoyance as a function of rotor–rotor axial spacing, for different number of blades, thrust setting and emission angle θ ($\theta = 180°$ on the left side, and $\theta = 90°$ on the right side).

Table 4
Pearson's Correlation coefficient r between reported annoyance and 5th percentile value of the SQMs Loudness (N5), Roughness (R5), Fluctuation Strength (FS5), Impulsiveness (I5) and Tonality (T5) for observer angles $\theta = 180°$ and $\theta = 90°$.

Sound Quality Metric	All	$\theta = 180°$	$\theta = 90°$
N5 (ANSI S3.4 FFT)	0.975**	0.957**	0.978**
R5 (Sottek's Hearing Model)	−0.077	−0.204	0.221
FS5	0.563**	0.822**	0.177
I5 (Sottek's Hearing Model)	−0.207	−0.278	−0.338
T5 (Sottek's Hearing Model)	0.590**	0.647**	0.511*

*Denotes p-values smaller than 0.05.
**Denotes p-values smaller than 0.01.

higher for 4 and 6 blades (26% and 29% respectively) than for 2 blades (12%). The increase in annoyance levels from 0.3 to 1.0 axial spacing is slightly higher for 2 and 4 blades, than for 6 blades, for both 4 N and 8 N.

At 90° emission angle (right side of Fig. 14), the values of reported annoyance seem to be independent from the rotor–rotor axial spacing, and no clear trend of noise annoyance is observed for different number of blades. The configurations with 6 blades seem to be perceived as less annoying than configurations with 2 and 4 blades for both 4 N and 8 N thrust.

The results shown in Fig. 14 seem to suggest that the reported annoyance at an emission angle of 180 degrees is driven by the effects of rotor–rotor interaction tones, whose radiation is maximum at this angle [6,7]. This seems to be confirmed by the results shown in Table 4, where a substantial correlation ($p < 0.01$) is observed between the reported annoyance and Loudness, Fluctuation Strength (accounting for beating effects between rotors' fundamental frequencies), and Tonality. Meanwhile, at an emission angle of 90 degrees, where there is a null in the directivity of all dominant sources, the reported annoyance correlates significantly with Loudness ($p < 0.01$) and with Tonality ($p < 0.05$). In summary, the annoyance levels in consequence of the operation of contra-rotating systems is highly dependent on the angle of emission considered. The annoyance levels reported by a receiver positioned on the axis of the contra-rotating system (at an emission angle of 180 degrees) will be highly influenced by the strength of rotor–rotor interaction tones. A receiver at other emission angles, where interaction tones radiate less efficiently, will likely base their annoyance responses on the effect of other dominant sources, such as rotor-alone noise. This is an important finding, as for aircraft carrying contra-rotating systems for Vertical Take-Off and Landing, a sub-optimal design of the rotor–rotor axial spacing will lead to an increase in loudness, tonality and "beating effects", and therefore an increase in noise annoyance at receivers beneath of the vehicle. It is important to note that take-off, landing and hover operating conditions of these aircraft could be the most challenging flight phases for noise annoyance due to the proximity of the aircraft to exposed communities.

6. Conclusions

This paper investigates the acoustic and psychoacoustics characteristics of small, contra-rotating propellers over a range of blade numbers and axial separation distances. Optimal configuration parameters for reduced noise have been determined, and a listening test was used to validate these configurations for reduced annoyance. The results reported in this paper contribute to the existing literature by (i) extending the acoustic and psychoacoustic analysis of contra-rotating systems to varying blade counts; (ii) investigating annoyance levels as a function of rotor–rotor axial spacing, blade count and emission angle. A key finding of this paper

is how annoyance levels are driven by different psychoacoustics factors at different emission angles, as the perceptually dominant noise source might change at each range of emission angles. These results can aid the optimisation of contra-rotating propellers, with a focus on minimising the noise annoyance due to vertical take-off and landing and hover operations of aircraft carrying contra-rotating systems.

Assuming identical thrust conditions, axial separation plays a critical role for both noise radiation and perceived annoyance, with optimal axial spacing – between $z/D = 0.2$ and 0.4 – showing minimum radiated noise levels, and a general balance between tonal and broadband noise. Sounds from these configurations were also rated less annoying, likely for these same reasons. The results presented herein are consistent with the current literature on noise from two-bladed contra-rotating propellers, and have been extended for higher propeller blade counts (3 to 6 blades) as well.

For larger axial spacings ($z/D > 0.3$), increasing the blade count at same thrust led to a reduction in tonal noise levels, and to a smaller extend to a reduction in broadband noise as well. These trends are similar to trends for single propellers, where higher blade counts have led to reduce noise at iso-thrust — possibly due to reduced blade loading and reduced rotational speed [19]. Reduced upstream rotor loading has been associated with weaker viscous wakes, leading to reduced wake-interaction noise at larger axial separations [20]. For closely spaced propellers ($z/D < 0.2$), higher blade counts lead to a significant increase in tonal noise levels due to increased potential field interaction.

Following the trends explained above, the regions of minimum level in the lower right corners of Fig. 4 and in Fig. 6 showed the proposed optimal axial spacing and number of blades for a contra-rotating propeller operating at constant 8 N thrust were ($z/D = 0.4$, 4 blades) when optimising for on-axis OASPL, and ($z/D = 0.3$, 5 blades) when optimising for the total Sound Power Level PWL. However, other configurations with similar axial spacings between $z/D = 0.2$–0.4 and 3–5 blades per rotor can all achieve similarly reduced OASPL and PWL. Therefore, there is a degree of flexibility in obtaining low-noise contra-rotating propeller configurations.

The Sound Power Level PWL is by nature a more robust optimisation metric than the sound radiated at a single emission angle, and can be useful when investigating trade-offs between very directive noise sources radiating at different emission angles. However, changes in Sound Power alone do not clearly reflect changes in directivity, and therefore both analyses are useful when evaluating complex aeroacoustic sources where competing noise generation mechanisms are present.

The findings of the psychoacoustic analysis presented can aid to find optimum configurations for low noise annoyance. For noise radiated on-axis, Loudness reaches a minimum at axial separations z/D = 0.3–0.4 for all blade counts; there is also a significant reduction in Tonality and Roughness as the axial spacing between rotors increases; and values of Fluctuation Strength lessen with axial spacing, especially for configurations with 2 blades. Increasing the number of blades leads to a reduction in Loudness and Roughness, but a small increase in Tonality. At 90° emission angle, no clear trend was observed in most of the SQMs evaluated due to the directivity null of both potential field interaction tones and broadband noise. In line with the acoustic analysis, the results of the listening experiment suggest that Annoyance is minimised at the optimal axial spacing $z/D = 0.3$ and higher blade counts. The reported noise annoyance is driven by Loudness, Fluctuation Strength and Tonality metrics ($p < 0.01$) at on-axis radiation, while at 90° emission angle Loudness ($p < 0.01$) and Tonality ($p < 0.05$) are the main contributors to noise annoyance.

A few factors not considered in the present work are the effects of varying advance ratios (i.e. non-zero inflow velocity), changes in propeller blade pitch, and other changes in the operating conditions. It is expected that the aerodynamic and aeroacoustic behaviour of the contra-rotating propellers presented herein will change significantly when tested in non-zero advance ratio, particularly regarding the dynamics of the convecting wakes and tip vortices, and these effects require further investigation. It has been observed that single propellers tend to be significantly noisier in static conditions than when in flight conditions (e.g. [32,33]), although it is unclear whether the same phenomenon applies to contra-rotating propellers, where most of the aerodynamic interaction is generated by the blade rows themselves. It has been proposed that the acoustically-optimal separation between propellers might also depend on the relative pitch angle between rotors [1,9], suggesting there might be an acoustically optimal pitch angle for a given rotor–rotor separation. Other changes in operating conditions, such as non-axial flight, are also expected to play a significant role on noise radiation by increasing unsteady blade loading [10]. All of the above factors could potentially change the importance of each noise generation mechanism to the overall acoustic radiation in unpredictable ways, and therefore require further investigation.

Declaration of competing interest

The authors declare that they have no known competing financial interests or personal relationships that could have appeared to influence the work reported in this paper.

Data availability

Data will be made available on request.

Acknowledgements

References

[1] R.S. McKay, M.J. Kingan, S.T. Go, R. Jung, Experimental and analytical investigation of contra-rotating multi-rotor UAV propeller noise, Appl. Acoust. 177 (2021) 107850, http://dx.doi.org/10.1016/j.apacoust.2020.107850, URL https://linkinghub.elsevier.com/retrieve/pii/S0003682X20309555.

[2] H. Bu, Z. Ma, S. Zhong, An experimental investigation of noise characteristics of overlapping propellers, J. Acoust. Soc. Am. 152 (1) (2022) 591–600, http://dx.doi.org/10.1121/10.0012735.

[3] E. Greenwood, K.S. Brentner, R.F. Rau, Z.F.T. Gan, Challenges and opportunities for low noise electric aircraft, Int. J. Aeroacoust. 21 (5–7) (2022) http://dx.doi.org/10.1177/1475472x221107377, 1475472X2211073.

[4] A.B. Parry, Theoretical Prediction of Counter-Rotating Propeller Noise (Ph.D. thesis), University of Leeds, 1988, URL https://core.ac.uk/download/pdf/43884.pdf.

[5] A. Filippone, Historical development of the coaxial contra-rotating propeller, Aeronaut. J. (2022) 1–38, http://dx.doi.org/10.1017/aer.2022.92.

[6] R.S. McKay, M.J. Kingan, R. Go, Experimental investigation of contra-rotating multi-rotor UAV propeller noise, in: Proceedings of ACOUSTICS 2019, Cape Schanck, Victoria, Australia, 2019, p. 10.

[7] A.J. Torija, P. Chaitanya, Z. Li, Psychoacoustic analysis of contra-rotating propeller noise for unmanned aerial vehicles, J. Acoust. Soc. Am. 149 (2) (2021) 835–846, http://dx.doi.org/10.1121/10.0003432, URL https://asa.scitation.org/doi/10.1121/10.0003432.

[8] A. Parry, M. Kingan, B. Tester, Relative importance of open rotor tone and broadband noise sources, in: 17th AIAA/CEAS Aeroacoustics Conference (32nd AIAA Aeroacoustics Conference), American Institute of Aeronautics and Astronautics, Portland, Oregon, 2011, http://dx.doi.org/10.2514/6.2011-2763, URL https://arc.aiaa.org/doi/10.2514/6.2011-2763.

[9] P. Chaitanya, P. Joseph, S. Prior, A. Parry, On the optimum separation distance for minimum noise of contra-rotating rotors, J. Sound Vib. 535 (2022) 117032, http://dx.doi.org/10.1016/j.jsv.2022.117032, URL https://linkinghub.elsevier.com/retrieve/pii/S0022460X22002504.

[10] D.A. Smith, A. Filippone, G.N. Barakos, Noise source analysis in counter-rotating open rotors, AIAA J. 60 (3) (2022) 1783–1796, http://dx.doi.org/10.2514/1.j060886.

[11] V.P. Blandeau, P.F. Joseph, Broadband noise due to rotor-wake/rotor interaction in contra-rotating open rotors, AIAA J. 48 (11) (2010) 2674–2686, http://dx.doi.org/10.2514/1.j050566, URL https://arc.aiaa.org/doi/10.2514/1.J050566.

[12] S.A. Rizzi, Toward reduced aircraft community noise impact via a perception-influenced design approach, in: Proceedings of Internoise, Hamburg, Germany, 2016, p. 25.

[13] S. Krishnamurthy, A. Christian, S.A. Rizzi, Psychoacoustic test to determine sound quality metric indicators of rotorcraft noise annoyance, in: INTER-NOISE and NOISE-CON Congress and Conference Proceedings, Chicago, IL, 2018, p. 12, URL https://www.ingentaconnect.com/content/ince/incecp/2018/00000258/00000007/art00032.

[14] M.A. Boucher, S. Krishnamurthy, A.W. Christian, S.A. Rizzi, Sound quality metric indicators of rotorcraft noise annoyance using multilevel analysis, J. Acoust. Soc. Am. 153 (2) (2023) 867–876, http://dx.doi.org/10.1121/10.0016888.

[15] A.J. Torija, Z. Li, P. Chaitanya, Psychoacoustic modelling of rotor noise, J. Acoust. Soc. Am. 151 (3) (2022) 1804–1815, http://dx.doi.org/10.1121/10.0009801, URL https://asa.scitation.org/doi/10.1121/10.0009801.

[16] F. Casagrande Hirono, A. Torija Martinez, A. Elliott, Optimization of a contra-rotating propeller rig for reduced psychoacoustic impact, in: Proceedings of Internoise, 2022.

[17] K.S. Brentner, F. Farassat, Modeling aerodynamically generated sound of helicopter rotors, Prog. Aerosp. Sci. 39 (2–3) (2003) 83–120, http://dx.doi.org/10.1016/S0376-0421(02)00068-4, URL https://linkinghub.elsevier.com/retrieve/pii/S0376042102000684.

[18] N.S. Zawodny, D.D. Boyd Jr., C.L. Burley, Acoustic characterization and prediction of representative, small-scale rotary-wing unmanned aircraft system components, in: Proceedings of AHS 72nd Annual Forum, West Palm Beach, FL, USA, 2016.

[19] R. Gojon, T. Jardin, H. Parisot-Dupuis, Experimental investigation of low Reynolds number rotor noise, J. Acoust. Soc. Am. 149 (6) (2021) 3813–3829, http://dx.doi.org/10.1121/10.0005068, URL https://asa.scitation.org/doi/10.1121/10.0005068.

[20] V.P. Blandeau, P.F. Joseph, M.J. Kingan, A.B. Parry, Broadband noise predictions from uninstalled contra-rotating open rotors, Int. J. Aeroacoust. 12 (3) (2013) 245–281, http://dx.doi.org/10.1260/1475-472x.12.3.245, URL http://journals.sagepub.com/doi/10.1260/1475-472X.12.3.245.

[21] R. Jung, M.J. Kingan, P. Dhopade, R.N. Sharma, Investigation of the interaction tones produced by a contra-rotating unmanned aerial vehicle propeller, in: 28th AIAA/CEAS Aeroacoustics 2022 Conference, American Institute of Aeronautics and Astronautics, 2022, http://dx.doi.org/10.2514/6.2022-2832.

[22] P. Virtanen, et al., SciPy 1.0: fundamental algorithms for scientific computing in Python, Nature Methods 17 (3) (2020) 261–272, http://dx.doi.org/10.1038/s41592-019-0686-2.

[23] S.A. Rizzi, D. Stephens, J.J. Berton, D.E. Van Zante, J. Wojno, T. Goerig, Auralization of flyover noise from open rotor engines using model scale test data, in: 20th AIAA/CEAS Aeroacoustics Conference, American Institute of Aeronautics and Astronautics, Atlanta, GA, 2014, http://dx.doi.org/10.2514/6.2014-2750, URL https://arc.aiaa.org/doi/10.2514/6.2014-2750.

[24] D.B. Stephens, H. Vold, Order tracking signal processing for open rotor acoustics, J. Sound Vib. 333 (16) (2014) 3818–3830, http://dx.doi.org/10.1016/j.jsv.2014.04.005, URL https://linkinghub.elsevier.com/retrieve/pii/S0022460X14002685.

[25] C.M. Ekoule, Advanced Open Rotor Far-Field Tone Noise (Ph.D. thesis), Faculty of Engineering and the Environment, Southampton, UK, 2017, URL http://eprints.soton.ac.uk/id/eprint/417819.

[26] A.D. Pierce, Acoustics: An Introduction to Its Physical Principles and Applications, third ed., Springer International Publishing, 2019, http://dx.doi.org/10.1007/978-3-030-11214-1, URL https://link.springer.com/book/10.1007/978-3-030-11214-1.

[27] H. Fastl, E. Zwicker, Psychoacoustics, Springer Berlin Heidelberg, Berlin, Heidelberg, 2007, http://dx.doi.org/10.1007/978-3-540-68888-4, URL http://link.springer.com/10.1007/978-3-540-68888-4.

[28] R. Sottek, Modelle zur Signalverarbeitung im Menschlichen Gehör (Ph.D. thesis), RWTH Aachen University, Aachen, Germany, 1993, URL https://publications.rwth-aachen.de/record/77398.

[29] ECMA, Standard ECMA-74: Measurement of Airborne Noise Emitted by Information Technology and Telecommunications Equipment, seventeenth ed., ECMA (European Association for Standardizing Information and Communication Systems), Geneva, Switzerland, 2019, URL https://www.ecma-international.org/publications-and-standards/standards/ecma-74/.

[30] A.J. Torija, I.H. Flindell, The subjective effect of low frequency content in road traffic noise, J. Acoust. Soc. Am. 137 (1) (2015) 189–198, http://dx.doi.org/10.1121/1.4904542.

[31] A.J. Torija, S. Roberts, R. Woodward, I.H. Flindell, A.R. McKenzie, R.H. Self, On the assessment of subjective response to tonal content of contemporary aircraft noise, Appl. Acoust. 146 (2019) 190–203, http://dx.doi.org/10.1016/j.apacoust.2018.11.015.

[32] B. Magliozzi, D. Hanson, R. Amiet, Propeller and propfan noise, in: H. Hubbard (Ed.), Aeroacoustics of Flight Vehicles: Theory and Practice, Vol. 1: Noise Sources, NASA (National Aeronautics and Space Administration), VA, USA, 1991, NASA-RP-1258-Vol-1. URL https://ntrs.nasa.gov/citations/19920001380.

[33] J. Whelchel, W.N. Alexander, N. Pisharoti, S. Brizzolara, R. Murali, D. Stilwell, Examination of broadband and tonal noise sources produced by eVTOL propellers and drive systems, in: 28th AIAA/CEAS Aeroacoustics 2022 Conference, American Institute of Aeronautics and Astronautics, 2022, http://dx.doi.org/10.2514/6.2022-3035.